AVCO EVERETT RESEARCH LABORATORY

a division of
AVCO CORPORATION

NONEQUILIBRIUM AND EQUILIBRIUM RADIATION AT SUPER-SATELLITE RE-ENTRY VELOCITIES

by R. A. Allen, P. H. Rose and J. C. Camm

RESEARCH REPORT 156
September 1962

HEADQUARTERS
BALLISTIC SYSTEMS DIVISION
AIR FORCE SYSTEMS COMMAND
UNITED STATES AIR FORCE
Contract No. AF 04(694)-33

NATIONAL AERONAUTICS AND SPACE ADMINISTRATION
MANNED SPACECRAFT CENTER
Technical Management Office
Houston, Texas

; Avco-Everett Res. Rept. -156;

; BSD-TDR-62-349) OTS:

RESEARCH REPORT 156

NONEQUILIBRIUM AND EQUILIBRIUM RADIATION AT SUPER-SATELLITE RE-ENTRY VELOCITIES

by

R. A. Allen, P. H. Rose and J. C. Camm

AVCO-EVERETT RESEARCH LABORATORY
a division of
AVCO CORPORATION
Everett, Massachusetts

[11]

September 1962 72p 50 refs

supported jointly by

HEADQUARTERS
BALLISTIC SYSTEMS DIVISION
AIR FORCE SYSTEMS COMMAND
UNITED STATES AIR FORCE
Air Force Unit Post Office
Los Angeles 45, California

under Contract No. AF 04(694)-33

NATIONAL AERONAUTICS AND SPACE ADMINISTRATION
MANNED SPACECRAFT CENTER
APOLLO PROCUREMENT OFFICE
Houston 1, Texas

(NASA under) Contract No. NAS 9-156

ABSTRACT

23019

Vehicles re-entering the Earth's atmosphere from lunar and interplanetary missions will encounter radiative heating significantly greater than was experienced by ICBM and satellite re-entry vehicles. An electric arc-driven shock tube has recently been developed which produces shock waves at super-satellite re-entry velocities. Photometric measurements of the radiation behind normal air shock waves have been made in this high performance shock tube, and the engineering estimates of the radiation heating derived from these measurements are described in this paper. Measurements were made of the nonequilibrium and equilibrium radiation from normal air shocks at initial pressures varying from 1.0 to 0.05 mm Hg, (Simulated altitudes 110,000 - 255,000 ft) and at shock velocities from 16,500 to 36,200 ft/sec. A calibrated grating, dual channel, monochromator and photomultipliers were used to obtain photometric measurements between .22 and .9 microns wavelength. A tungsten photoelectric gauge was used to obtain quantitative intensity results in the 0.075 - .14 micron region and a single channel prism monochromator with an infrared cell was used to obtain coverage at wavelengths beyond 1.0 micron. From time histories of the resolved shock front radiation at various wavelengths and at various velocities and pressures, a parametric description of the radiation was obtained. Quantitative equilibrium and integrated nonequilibrium radiation intensities, the width of the nonequilibrium region, and the time required by the radiation to peak behind the shock front have been measured. This parametric study validated "binary scaling" of the nonequilibrium radiation. The $N_2^+(1-)$ system and atomic nitrogen lines have been identified to be significant contributors to both the equilibrium and nonequilibrium radiation at 33,000 ft/sec at initial pressure of 0.1 mm Hg. A continuum background has been observed and attributed to Kramers' radiation produced mainly by the capture of electrons by nitrogen atoms ions. A summary of existing data between 0.075 and 2.7μ indicates an approximate upper bound for nonequilibrium radiation of 40 watts/cm^2 - 2π ster. at 33,000 ft/sec. Currently, it is not possible to accurately predict nonequilibrium radiation from a given normal shock wave at high velocities. The present state of the theoretical knowledge of nonequilibrium and equilibrium radiation and methods of folding experimental results into flow calculations are summarized. Finally, the engineering implications of the radiation results presented are explored.

Author

I. INTRODUCTION

For the past several years, heat transfer of re-entry velocities of up to 25,000 ft/sec have been thoroughly explored.[1-4] For increasingly higher re-entry velocities, the radiative heating becomes a larger fraction of the over-all heat flux, and some feasible flight paths above escape velocity are such that the radiative heating could be the dominant heat flux.[3, 5, 6]

The radiative properties of high temperature air have been shown to be dominated by the radiation from the molecular bands of nitrogen, oxygen and nitrogen oxide, and the molecular and atomic ions.[7, 8] These species undergo vast excursions in their concentrations during the approach to the equilibrium state behind a normal shock and, consequently, it is no surprise that the radiative history of normal shock waves also marks this behavior. It has been shown that under certain conditions, the radiative energy release during the relaxation process behind the shock front can result in the transport of significant quantities of energy. As a result of the identification of this source of radiant energy, the study of radiative energy transport has generally been divided into equilibrium and nonequilibrium radiation, referring to the properties of the after and before the gas has relaxed to the thermodynamic equilibrium state after a normal shock, respectively.

At velocities of 30,000 to 40,000 ft/sec, the translational temperature immediately behind the shock front may be as high as 40,000 to

to 75,000°K. If only the translational and rotational degree of freedom is excited in the air immediately behind the shock front, this translational temperature is given by the Rankine-Hugoniot relationships for $\gamma = 7/5$. However, this temperature is quickly reduced as the chemical and vibrational processes occur in the relaxation region behind the shock front. Due to the coupling between molecular electronic excitation and the thermodynamic condition of the gas, the molecular radiation in this relaxation region shows the considerable overshoot in intensity above the equilibrium level.

The chemical and excitation processes occurring during this non-equilibrium or relaxation region are dominantly binary reactions, i.e., the results of two-body collisions. It follows that the intensity of radiation from such reactions should be proportional to the particle density, and the thickness of the region should be inversely proportional to the density. Consequently, as long as binary mechanisms predominate, the integrated radiation flux emitted from such a nonequilibrium region should be independent of density at a given velocity. Experimental verification of binary scaling of the luminous front radiation was given in Refs. 5 and 9. It is also demonstrated by data collected in this study. The thickness of the nonequilibrium region and the time required for the radiation to reach its peak intensity are shown to scale as binary phenomena.

There are four effects, predictable from the physics of radiative processes, which may depress either the nonequilibrium or equilibrium radiation energy transport to a body, and thus invalidate binary scaling. Truncation, as discussed by Teare,[9] occurs when the width of the

nonequilibrium region is thicker than the shock detachment distance. Collision limiting[7] reduces the radiation intensity at low densities when the particle density in the gas is so low that there are not sufficient collisions to maintain the population of excited states against the drainage by radiation. Radiation cooling[9] occurs when the energy loss by radiation becomes an appreciable fraction of the total energy of the flow. Under the nonequilibrium conditions, this phenomenon occurs at low densities where the flow energy is small. Equilibrium radiation increases with body size and is proportional to more than the first power of density, and consequently radiation cooling by equilibrium radiation is most significant for large bodies and at high densities. The fourth effect is the fact that under some conditions, the gas may not be optically thin. When the total radiation intensity of an optically thin gas exceeds 10% of the black body value, it is necessary to consider reabsorption in the gas.[10]

The total radiative flux to a body is the sum of the integrated nonequilibrium radiation and the equilibrium flux. Equilibrium radiation from air in the temperature and density range of interest to super-satellite re-entry velocities varies approximately as the 1.7 power of the density. Nonequilibrium radiation, however, is invariant with density due to binary scaling. The body size effects equilibrium intensity by changing the thickness of the radiating layer but has no effect on the nonequilibrium contribution. Thus, a density should be reached at high altitudes and small body sizes , where the nonequilibrium radiation exceeds the equilibrium value. The density at which equilibrium and nonequilibrium radiation intensities are equal will vary with the body size to the 1/1.7 power.

A point is reached at high altitudes where the shock detachment distance is smaller than the distance necessary for the gas to relax to equilibrium behind the shock front. If the ambient density where this occurs is low enough (i.e., large nose radii), there will be a "luminous front plateau" extending between this altitude and the altitude at which the nonequilibrium intensity became the dominant contribution. Over this altitude range, the integrated total radiation intensity remains constant despite the fact that the thickness of the nonequilibrium region varies. For small nose radii, this "luminous front plateau" will cover a smaller density range since this "truncation" starts to occur at high densities.

As the nonequilibrium region of the shock front becomes smaller than the characteristic flow length, truncation gradually starts to decrease the total integrated nonequilibrium radiation. When the characteristic distance is equal to the radiation peak, the integrated radiation starts to fall off rapidly, varying approximately as the square of the density as a consequence of the binary scaling of the radiation profile.

A fall-off in the luminous front plateau also occurs at low densities due to "collision limiting" which vitiates the binary scaling in the shock front. Collision limiting for a large body would cause the integrated radiation intensity to vary linearly with density, whereas severe truncation of a binary scaled region would introduce a density squared dependence.

At present, no adequate theory exists which enables accurate calculations of the luminous front radiation. However, by using general principles in conjunction with the present experiments at appropriate velocities, good estimates of the radiation heat fluxes for super-satellite re-entry

velocities can be made. This paper covers both experimental and theo - retical work on the nonequilibrium radiation problem in the 35, 000 ft/sec speed range. The electric arc-driven shock tube has been used to produce shocks of this velocity. The major part of the experimental data was obtained by photometry using a calibrated monochromator with photomulti - pliers, or photoconducting infrared cells. Vacuum ultraviolet, integrated radiation measurements were taken with a tungsten photoelectric gauge. These measurements along with a theoretical analysis of the equilibrium radiation are summarized. An empirical calculation scheme for the non-equilibrium radiation is developed and is incorporated into a flow field calculation for a two-foot nose radius flying at 35, 000 ft/sec.

II. ELECTRIC ARC-DRIVEN SHOCK TUBE

Normal shock waves with speeds up to satellite velocities have been produced for a number of years in combustion-driven shock tubes.[11] These shock tubes have proved invaluable in preparing a gas sample for study under conditions simulating gaseous phenomenon occurring during missile and satellite re-entry into the Earth's atmosphere. Simulation of the phenomena produced by the re-entry of space probes at escape velocities, however, is beyond the capabilities of conventional cumbustion-driven shock tubes.

Recently, an electric arc-driven shock tube has been developed[12] which is capable of producing normal shocks with good test time at velocities in excess of escape velocity.

A schematic diagram of an electric arc-driven shock tube is presented in Fig. 1. The driver section is made of a 1-1/2-inch inside diameter stainless steel tubing lined with a 3/32-inch thick teflon insulator. The driver is separated from the low pressure test gas section by a conventional stainless steel diaphragm which may also be used an an electrode. The other end of the driver is closed with a copper electrode which is supported by a nylon insulator. A fine aluminum wire is stretched between a hole in the center of the copper electrode and the diaphragm end of the driver.

Each capacitor is connected to collector plates by a coaxial cable. The ground plate is connected to the driver body. The high voltage terminal is connected to the copper electrode through a lovotron switch mounted

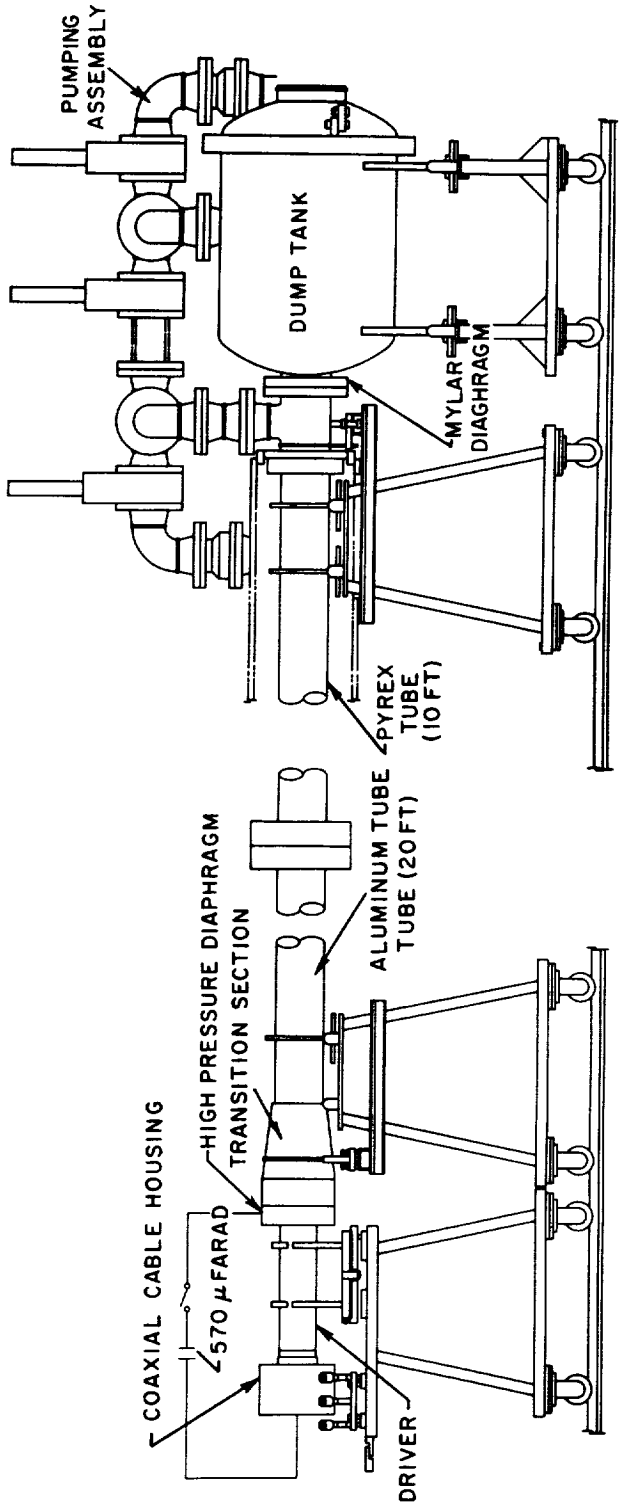

Fig. 1 Schematic diagram of typical arc-driven shock tube. This shock tube is identical to a combustion-driven shock tube except for the method of energy addition in the driver.

on the high voltage plate.

For a typical run, the driver is evacuated and then filled with helium to a pressure of 200 psi. The capacitor bank is charged to 18 KV. By energizing the lovotron switch, the capacitor bank is connected directly across the driver electrodes. The starter wire explodes and initiates an arc in the helium. The capacitor bank discharges through the helium in about 40μsecs, heating it to a temperature of the order of 20,000°K. The diaphragm-electrode breaks approximately when the helium reaches its peak pressure, approximately 10,000 psi, and the driver gas expands into the low pressure air test section, driving a shock wave before it. The details regarding the operation and performance of this device have been thoroughly described in Ref. 12.

III. MONOCHROMATOR MEASUREMENTS

A. Monochromator

Photometric measurements were made in the wavelength range of .24 to .90μ using a dual channel Bausch and Lomb grating monochromator having quartz optics. The arrangement of the equipment was identical to that described by Allen, Camm and Keck,[13] and is shown schematically in Fig. 2. The monochromator was equipped with three photomultipliers; two of these measured the radiation intensity in two adjacent narrow wavelength bands selected by the monochromator, and the third monitored a fraction of the total radiation passing through the entrance slit.

Typical oscillograms of the output of the photomultipliers are shown in Fig. 3. The measurements were made in the .55 to 1.0μ and .40 to .42μ wavelength regions at three different velocities and an initial pressure of 0.1 mm Hg. The time resolution of the optical system used was approximately 0.1 μsec. This resolution was achieved by using a 0.5mm wide monochromator entrance slit in conjunction with appropriate stops. The measurements were made looking through quartz ports mounted in copper knife edges which protruded into the center of the shock tube to eliminate boundary layer effects along the shock tube walls and shock curvature.[14]

Calibration of the complete optical train, including the appropriate filters to prevent overlapping of orders, was made using both a standard tungsten ribbon filament lamp and a graphite arc. The brightness temperature of the standard lamp was given as a function of lamp current at

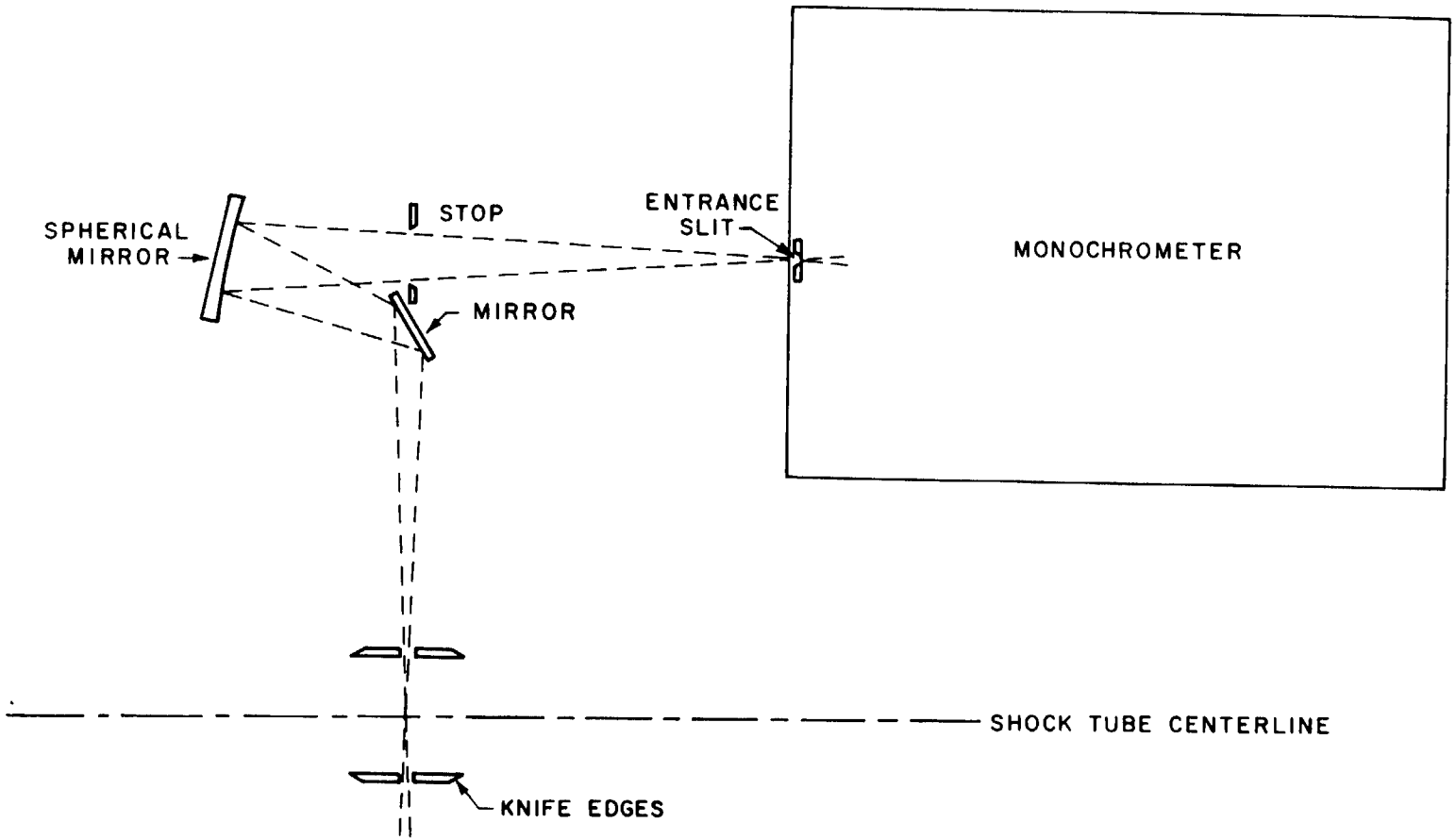

Fig. 2 Schematic diagram of monochromator and optical train used to obtain incident shock measurements. The knife edges are used to reduce boundary layer effects.

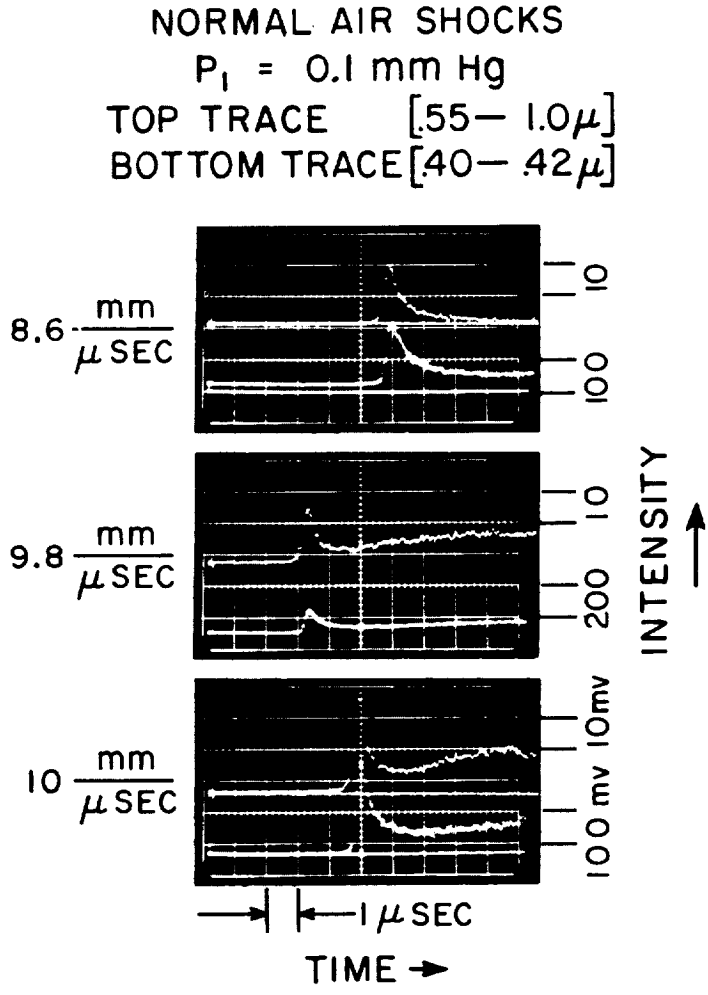

Fig. 3 Oscillogram records of radiation behind normal shocks in air at various shock velocities. The relatively level region behind the radiative overshoot region is taken as the equilibrium region.

a wavelength of .653μ by the National Bureau of Standards. The spectral intensity of the lamp at other wavelengths was calculated using data on the emissivity of tungsten given by DeVos[15] and the transmission of the quartz window. The arc was used to calibrate at shorter wavelengths. Data on the true temperature and spectral emissivity of such arcs has been given by Euler.[16] In the region of overlap between the tungsten lamp and the arc, the two methods of calibration agree within 20% or better. The wavelength scale of the monochromator was calibrated with a mercury lamp. The error in setting the monochromator was estimated to be about $\pm$ 5 Å .

A single channel Perkin-Elmer infrared monochromator was used to make measurements beyond 1μ. The schematic diagram of this monochromator and optical train is the same as that shown in Fig. 2. The image of the monochromator entrance slit was focused at the axis of the shock tube with the solid angle determined by the limiting stops. Care was taken that the port hole did not limit the solid angle since this would introduce an appreciable calibration error into the results. The light from the exit slit was collected and focused on the detector surface by a Cassegrain optical system mounted on the monochromator.

For the measurements between 1.0 and 3.0μ, the monochromator was equipped with a calcium fluoride prism. The detector used in the 1.0μ to 1.5μ wavelength region is a M7500 Germanium photodiode manufactured by Texas Instruments, Inc. The output of the detector was coupled to an amplifier by a cathode follower, the output of which was recorded by dual beam oscilloscopes. A liquid-nitrogen cooled, gold doped germanium detector was used beyond 1.5μ.

B. Equilibrium Radiation Measurements

Data on the equilibrium intensity of radiation from normal air shocks at 10 mm/μsec at an initial pressure of 0.1 mm Hg are shown in Fig. 4, as deduced from the level position of the profiles shown in Fig. 3. The slight rise in equilibrium radiation as one moves away from the shock front has been attributed to effects of attenuation of the shock velocity as it moves down the tube.[17] All the experimental data were obtained at the same shock speed within 3%, producing an equilibrium temperature of 9650°K $\pm$ 250° and about 10% $\pm$ 2% ionization. The two intensities obtained in adjacent channels with the Bausch and Lomb monochromator on a particular run are represented by a solid triangle and open circle connected by a short line. The wavelength resolution between 1.0 and 2.0μ of the single channel Perkin-Elmer monochromator measurements is indicated in the figure.

The prominent features of these equilibrium measurements are the N and O line contributions between 0.6 and 1.5μ and the $N_2^+(1-)$ molecular band system between 0.3 and 0.5μ. These atomic lines have previously been identified spectroscopically in reflected shocks[7] but not measured quantitatively.

The velocity and density dependence of the equilibrium radiation measurements are shown in Fig. 5. Several representative wavelength regions were chosen and data was obtained at various velocities and densities. Theoretical curves were constructed for the known important radiating species as discussed later. The data presented overlap with conventional combustion-driven shock tube results at lower velocities.[7]

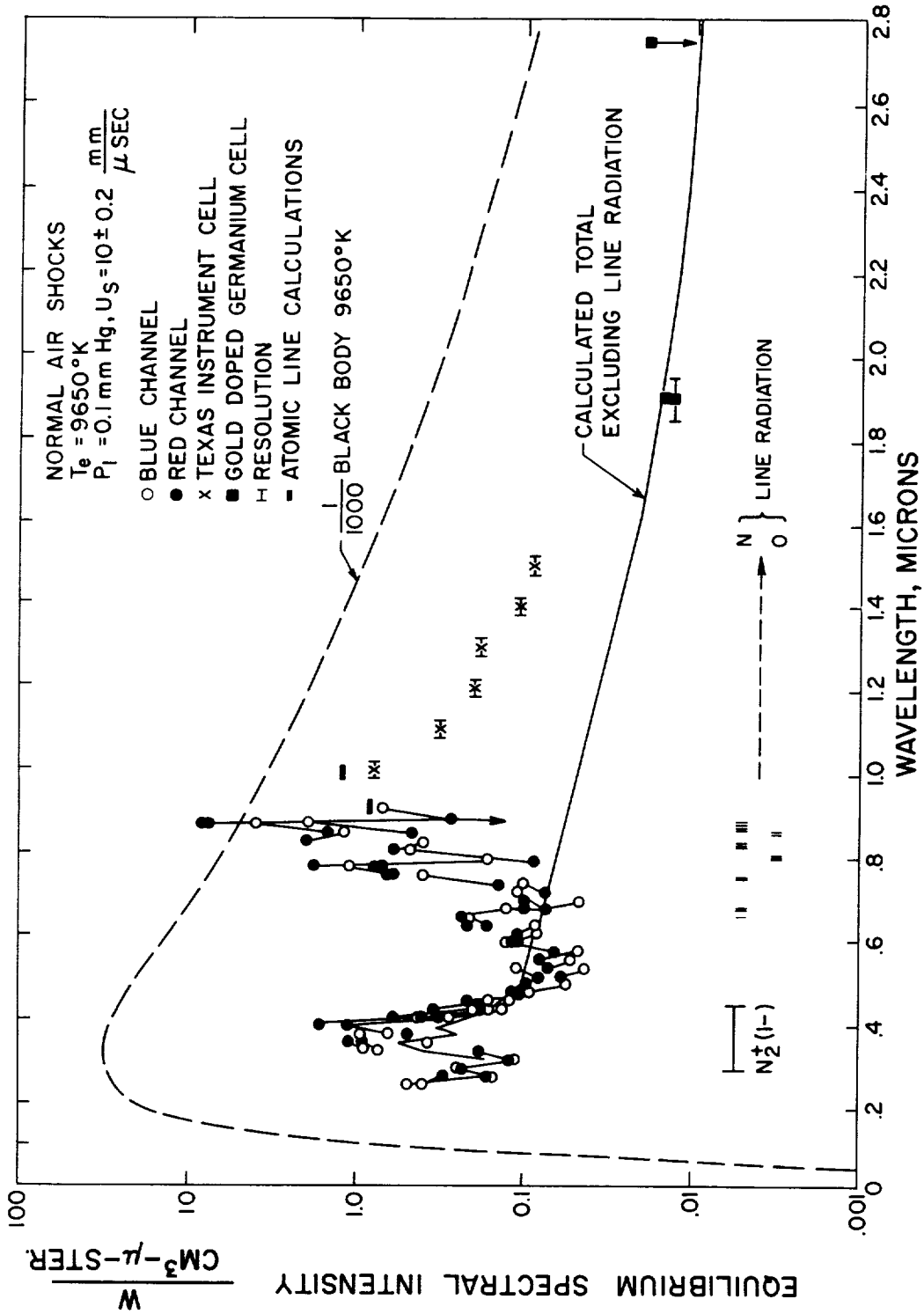

Fig. 4 Equilibrium radiation data obtained by photomultipliers and infrared gauges versus wavelength obtained on incident air shocks U_s = 10 mm/μsec, P_1 = 0.1 mm Hg. The degree of ionization is about 10%.

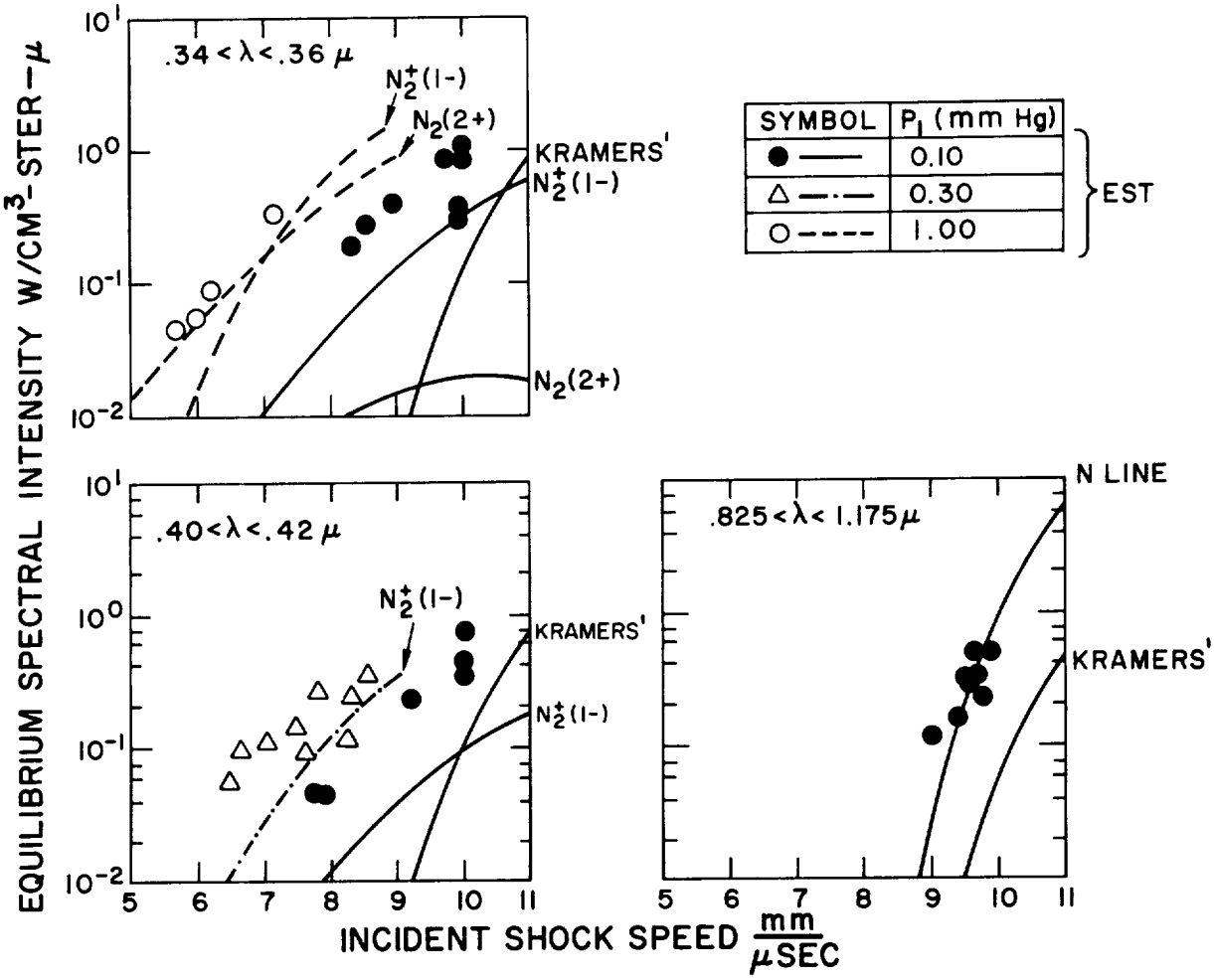

Fig. 5 Equilibrium radiation measurements behind normal air shocks at various initial pressures and shock velocities. Sets of measurements were made in the indicated wavelength intervals. Theory curves are constructed using published values for f numbers.

C. Nonequilibrium Radiation Measurements

Measurements of the nonequilibrium radiation were made by detailed examination of radiation profiles such as those shown in Fig. 3. The total nonequilibrium radiation was obtained from integration of the area under the luminous front profile. The point where the radiation intensity was observed to have fallen to a level 10% above the equilibrium level[18] was used to define the width of the nonequilibrium regions, called $d_{0.1}$. When the integration of the profile is converted from a laboratory fixed coordinate system to particle time, the units of the radiation intensity measurement, i.e., watts/cm^2 - ster - μ become watts/cm^2 - ster μ. Multiplying the data by 2π steradians gives the integrated luminous front radiation intensity from one side of an infinite slab.

Measurements from a shock speed of 33,000 ft/sec, and an initial pressure of 0.1 mm Hg, are shown as a function of wavelength in Fig. 6. The wavelength region covered by the monochromator and photomultipliers extended from 0.21 μ to 2.0 μ. The measurements plotted at a wavelength of 0.1 μ will be discussed later.

The total integrated luminous front radiation can be obtained from this graph by determining the area encompassed by the data points. A dashed line was drawn as an upper edge of a generous envelope including all the data points. The area under this dashed curve is 40 watts/cm^2 - 2π ster. In regions where the least measurements are available, and where large contributions could physically originate, the dashed line was drawn purposely high. Atomic lines are noticed to contribute appreciably to the integrated nonequilibrium radiation.

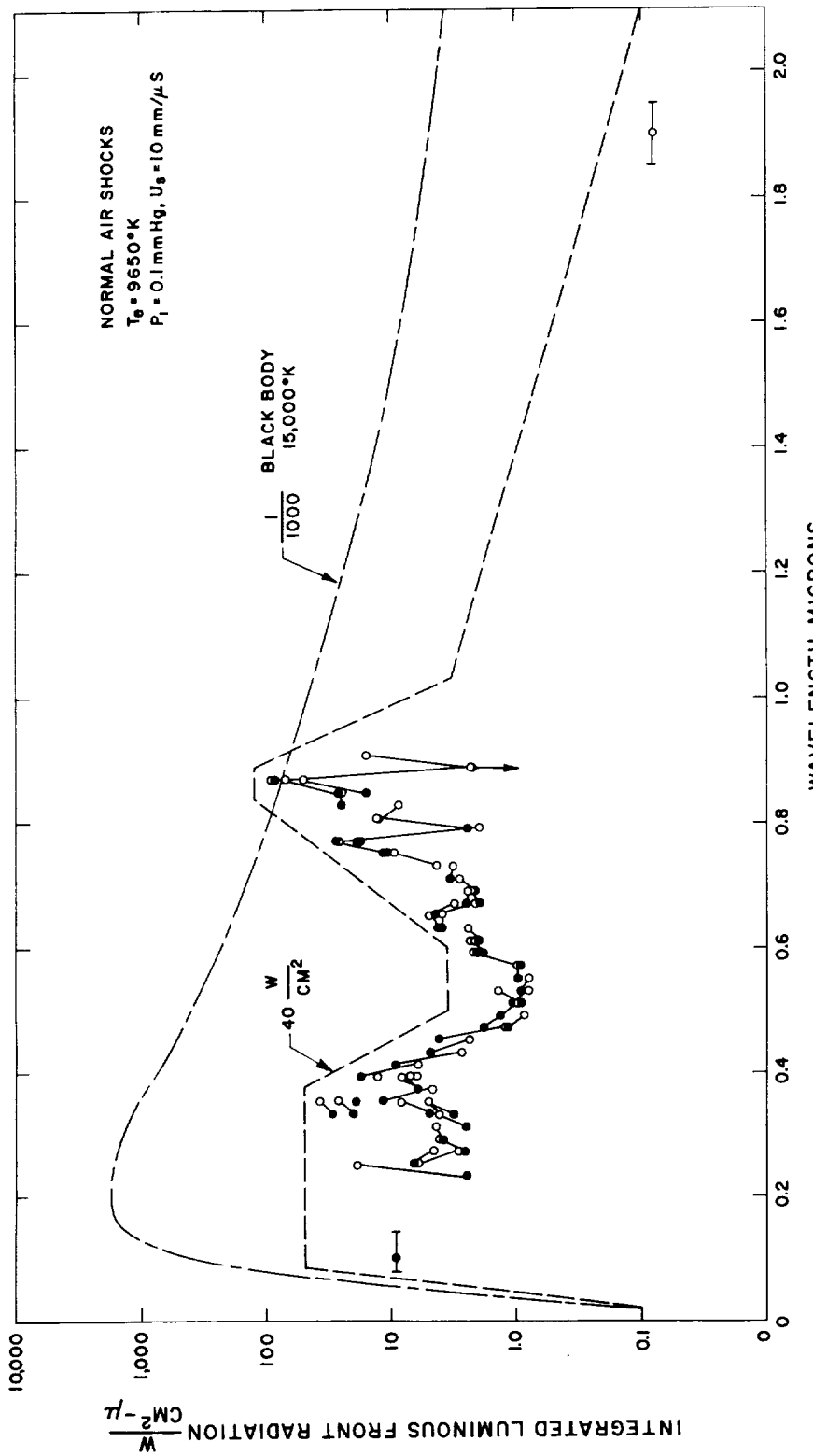

Fig. 6 Nonequilibrium radiation measurements of normal air shocks versus wavelength. The shock conditions are U_s = 10 mm/μsec, P_1 = 0.1 mm Hg. The area under the dashed curve is 40 watts/cm^2 - 2 π ster.

The absolute intensities of the radiation at the time of radiation peak at various wavelengths are shown in Fig. 7. The peak intensities demonstrate clearly that the atomic lines are prominent in the non-equilibrium region. The ratios of intensity at the nonequilibrium peak, I_P, to the equilibrium intensity, I_P/I_e, is shown as a function of wavelength in Fig. 8. The average peak to equilibrium ratio at these conditions was approximately four. There was no overshoot observed at the wavelength of 1.9 microns. The atomic line radiation and the $N_2^+(1-)$ system overshoots, but the latter is low relative to other wavelengths. This is not completely unexpected since the activation energy of this system is relatively small compared to other molecular radiators, and since nitrogen ions must first be produced in the nonequilibrium region before any radiation from this system can be observed. Thus, the nitrogen ions may have a longer excitation time than the molecular bands.

The velocity and density dependence of the radiation at representative wavelengths is presented in Fig. 9 for initial pressures varying from 0.05 to 1.0 mm Hg. If binary mechanisms dominate and there is no collision limiting in the nonequilibrium region, the integrated luminous front radiation should be independent of density. This fact is reasonably well borne out by data presented in this figure.

The time required for the luminous front intensity to fall to a level 10% above the equilibrium value has been defined as a measure of the nonequilibrium distance. The time to this level, called $t_{0.1}$, measured in the laboratory coordinate system, multiplied by the shock velocity, U_s, gives the distance to this level in the particle fixed

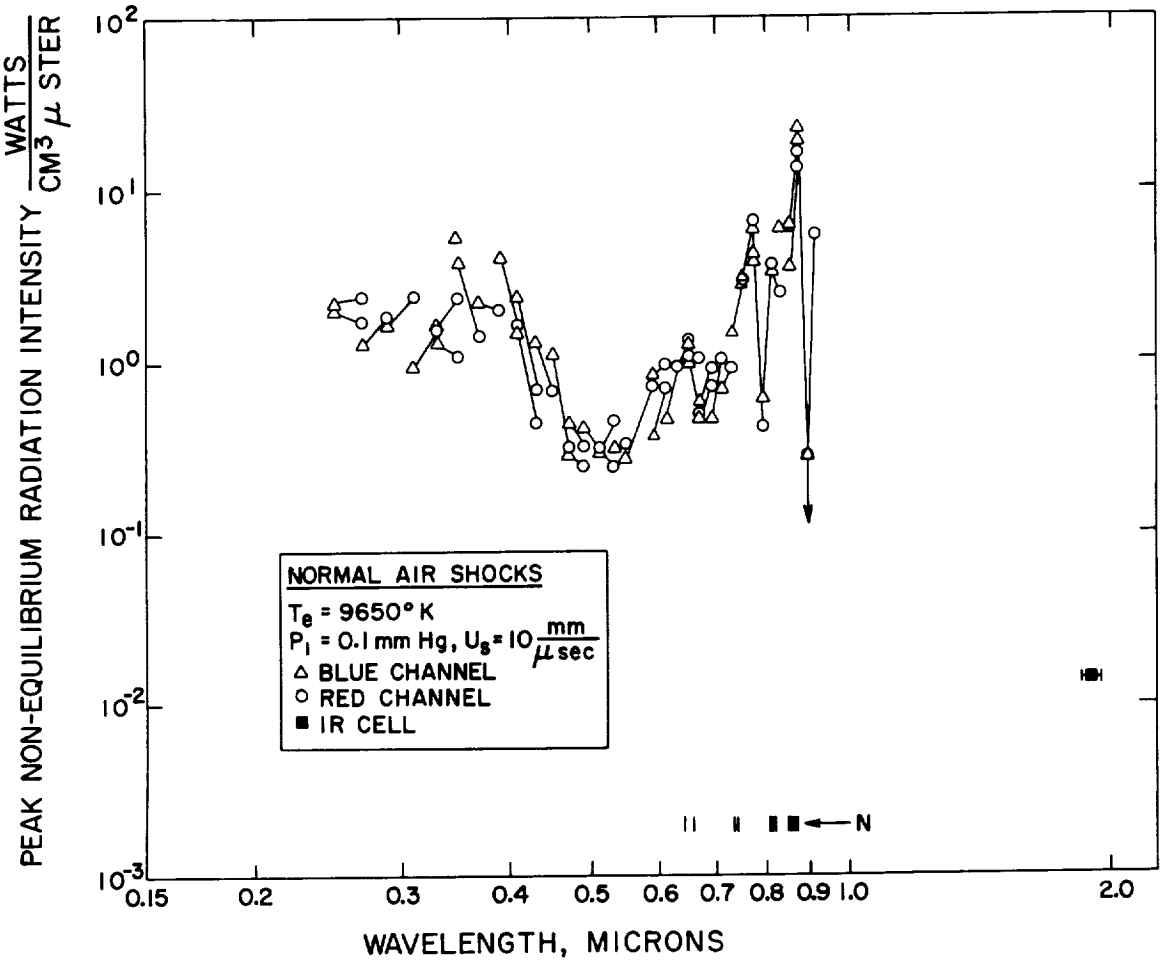

Fig. 7 Absolute intensity measurements versus wavelength at the time of peak radiation.

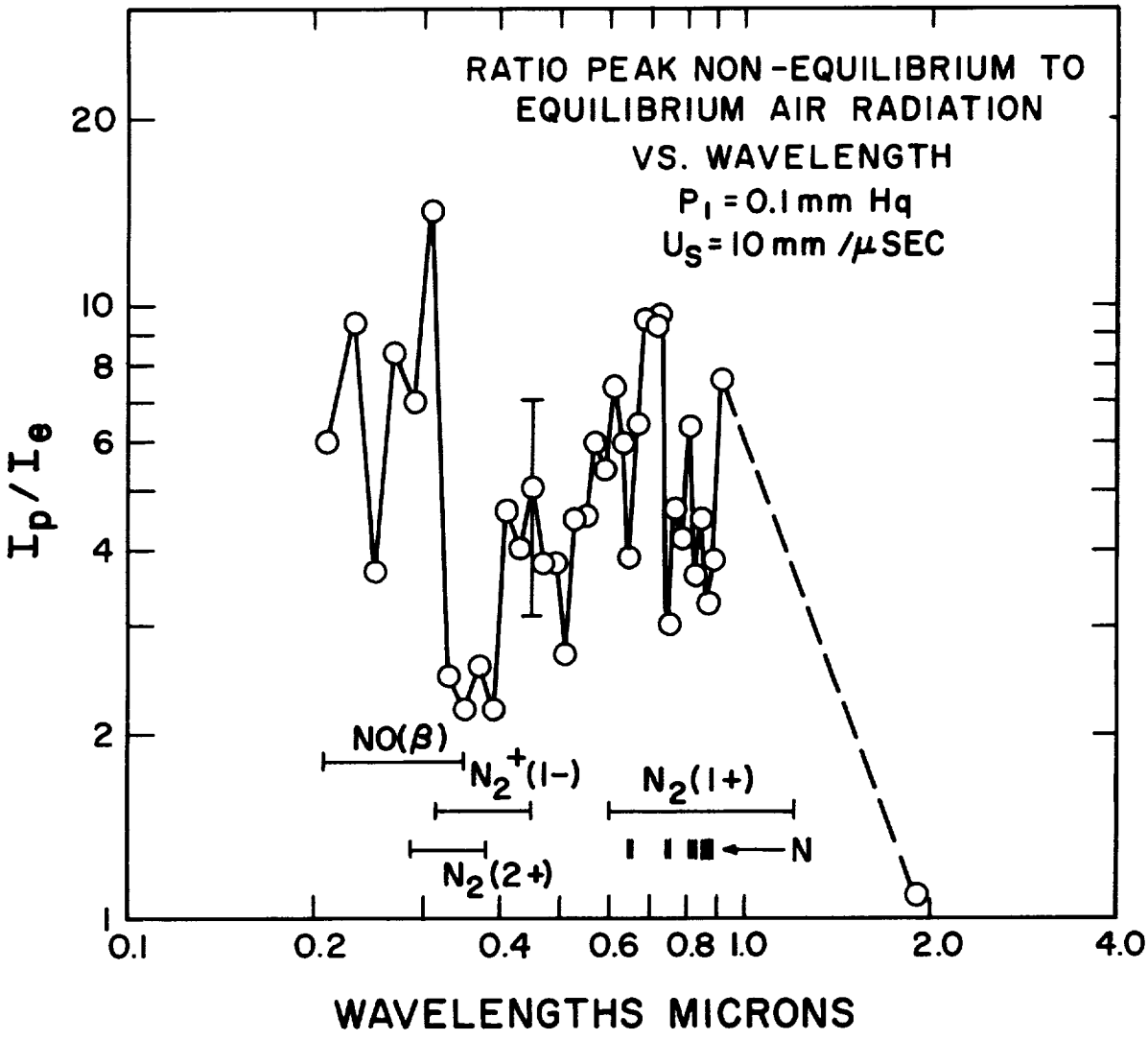

Fig. 8 Ratio of peak nonequilibrium to equilibrium radiation versus wavelength. No overshoot was observed in the measurement at 2.0 μ.

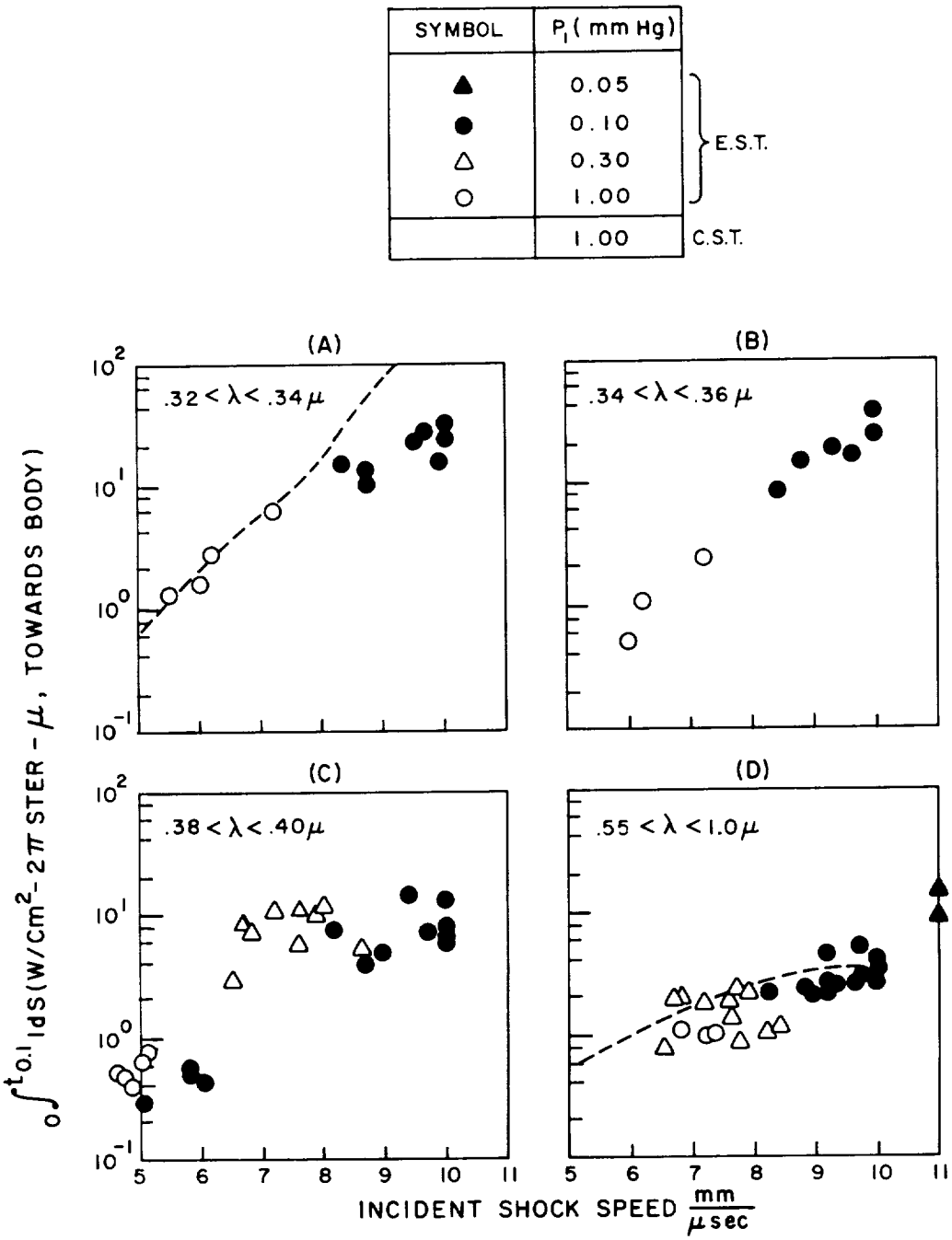

Fig. 9 Nonequilibrium radiation measurements of normal air shocks at various initial pressures and shock velocities. Sets of measurements were made in the indicated wavelength intervals. The dashed lines in A and D are based on the empirical calculation scheme discussed in the text.

coordinate system, i.e., $d_{0.1} = t_{0.1} U_s$. In like manner, the distance to the peak radiation, d_p is $U_s t_p$, where t_p is the time to peak radiation. Values of $t_{0.1}$ and t_p are presented as functions of shock velocity in Fig. 10. Measurements made at different initial pressures are presented here on a single plot whose ordinate is the product of pressure and time, i.e., $P_1 t$. This product should be approximately independent of initial pressure in a binary regime.

Over the small range of initial pressures covered by these experiments, a single curve could be drawn through each of the two sets of data (the solid and dashed lines in Fig. 10). From these two curves, nonequilibrium distance, $d_{0.1}$, and peak radiation distance, d_p, can be calculated for various velocities.

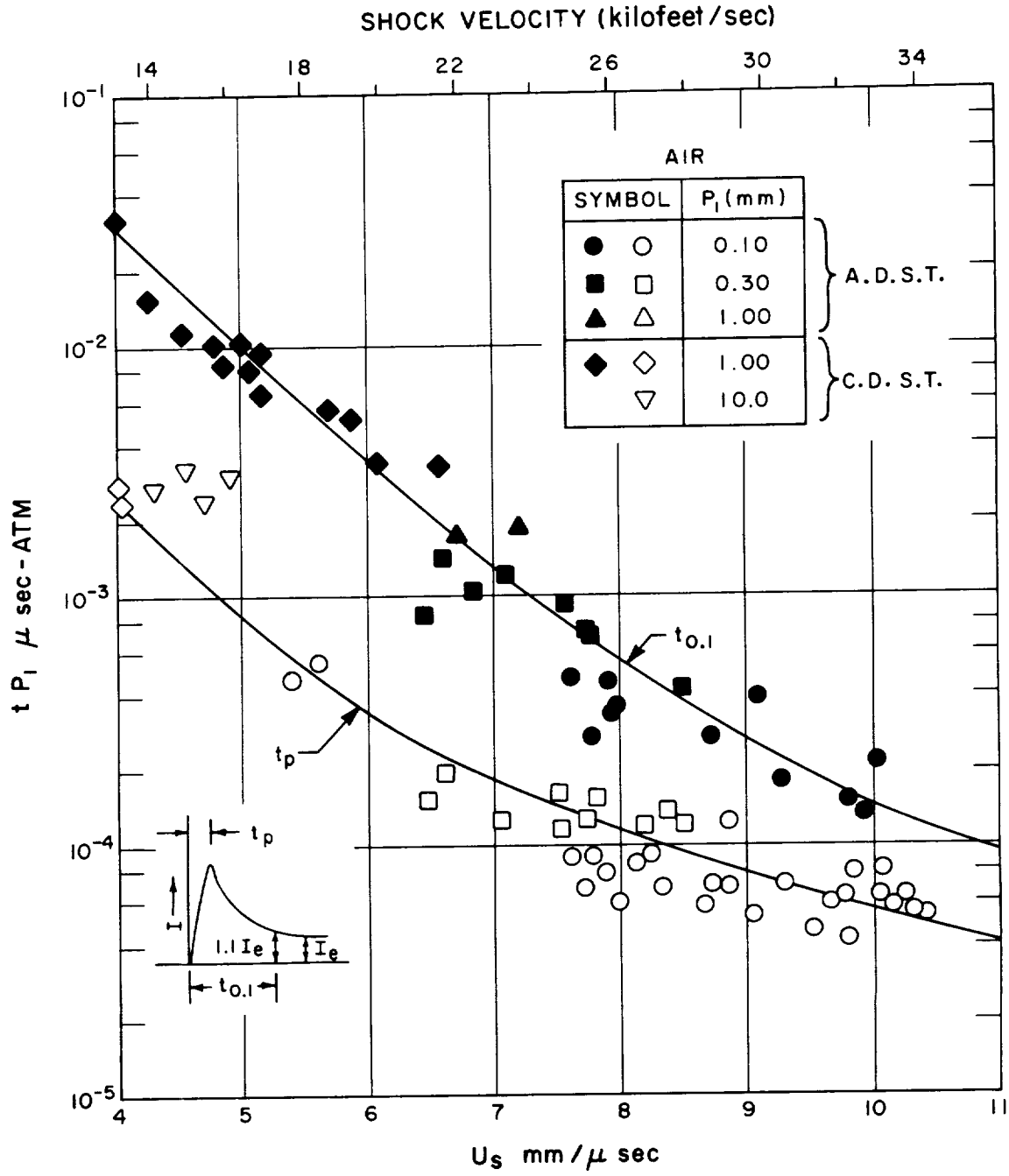

Fig. 10 Observed time duration of luminous front and time to peak in air plotted versus shock speed. The time $t_{0.1}$, in the laboratory coordinate system, is taken to a point at which the radiation intensity has decayed to a level 10% above equilibrium. Initial pressure is used as a scaling factor to correlate data obtained at different values of P_1. The solid and dashed curves are empirical fits.

IV. PHOTOELECTRIC GAUGE MEASUREMENT

Measurements have been made of the nonequilibrium radiation intensity from a 10 mm/μsec normal shock in air at a pressure of 0.1 mm of Hg in the wavelength region of from .075 to .14μ using a tungsten photoelectric gauge.

Preliminary tests were made to see where in the shock tube, the ultraviolet radiation originated. A tungsten photoelectric gauge was placed on the axis of the shock tube facing the driver with a 1-1/2-inch steel disk supported coaxially at a distance of 7/8-inch in front of the gauge. The time at which the shock struck the disk was clearly indicated by the time the trace goes off scale. This sudden rise was due to radiation from the shock reflected from the disk. The oscillograms from 10 mm/μsec shocks showed that the ultraviolet radiation began to appear about 8.6μsec before the shock struck the disk. This time corresponded to the point where the shock began to enter the field of view of the gauge. This test clearly indicated that the source of the measured ultraviolet radiation was the shock-heated air, not the driver gas. Since the temperature in the nonequilibrium region is many times that in the equilibrium region, it has been assumed that the radiation came from the nonequilibrium region.

The construction details of the photoelectric gauge and its operating principles were described in Ref. 5. Briefly, it consists of a 3/8-inch diameter tungsten disk supported coaxially in a shock tube and masked by its cylindrical case to include a field of view of about 53^{o}. The gauge was

held at a negative potential of about 30 volts and the photoelectric current was measured across a 2200 ohm load resistor as the shock approached. The 53^{o} field of view should provide a period of 14 sec when the gauge irradiation is constant, provided there is no appreciable absorption in the test gas between the gauge and the shock. A typical oscillogram is shown in Fig. 11 . The fact that the plateau was absent from the oscillogram indicates that the absorption was strong at distances as small as 3/8-inch.

In order to interpret the measurement, the spectral distribution of the source must be assumed. If the radiating species in the region over which tungsten is sensitive is assumed to be the nitrogen Worley bands $(b'^{1}\ \Sigma_{u}^{+} \rightarrow X^{1}\ \Sigma)$[19] then the spectral intensity should be proportional to $1/\lambda^{5}$ between 0.8 to .13 microns. Making this assumption and using the response of the gauge at the instant when the shock hits, a spectral intensity was computed as shown in Fig. 11. The integrated value of the spectral intensity curve was found to give a total radiation intensity in this region of 0.1 watts/cm^{2} - ster. This value corresponds to a value of 9.4 w/cm^{2} - micron radiating towards the body. This value was shown along with the monochromator data in Fig. 6.

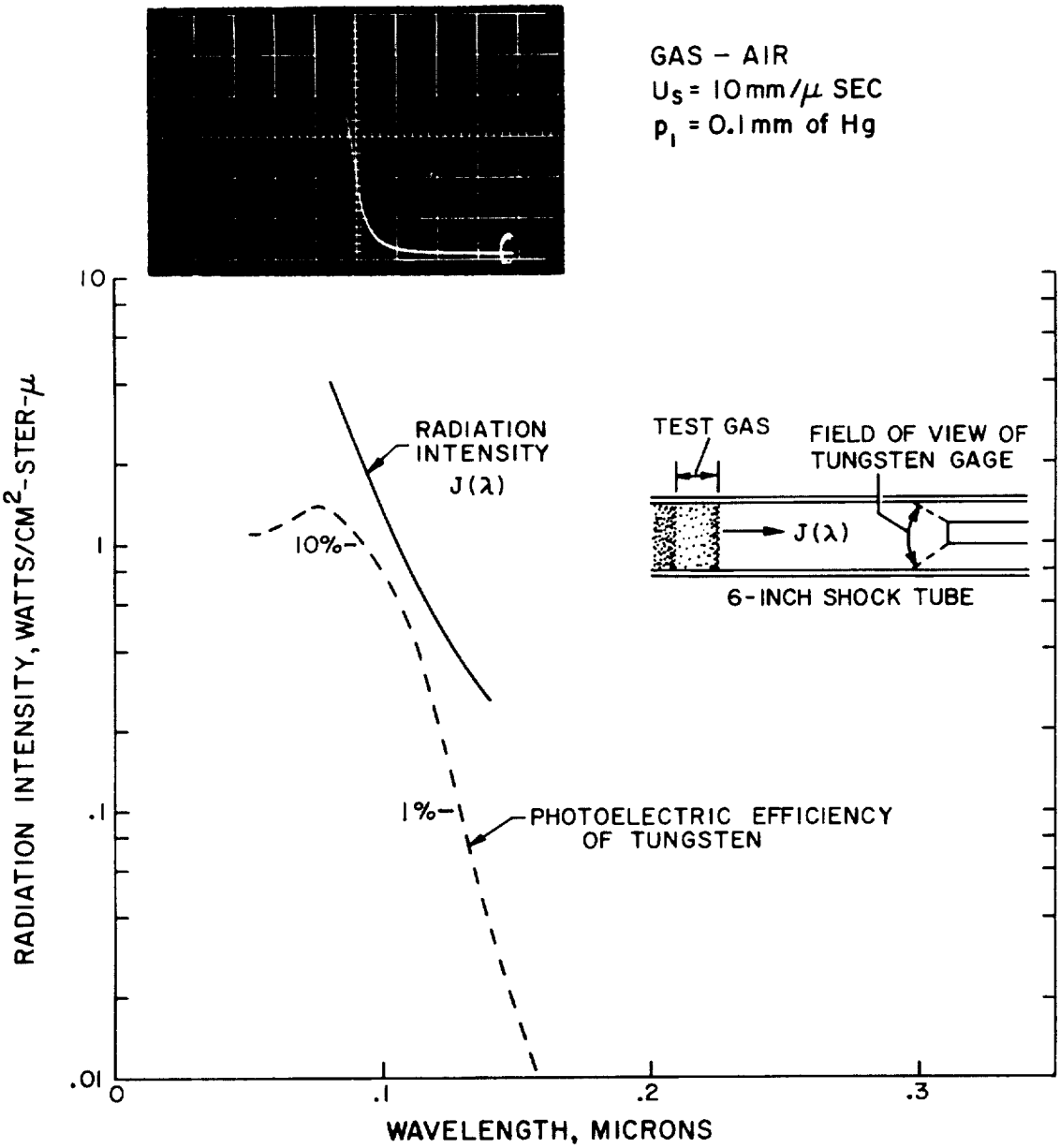

Fig. 11 Spectral intensity of the ultraviolet radiation from a 10 mm/μ sec shock in air at a pressure of 0.1 mm of Hg assuming a λ^{-5} distribution from .08 to 0.13μ; spectral photoelectric efficiency of tungsten; and oscillogram showing the gauge response as the shock approached.

V. EQUILIBRIUM RADIATION CALCULATIONS AND COMPARISON WITH DATA

A. Kramers' Radiation

It is evident that for incident shock velocities in excess of approximately 9 mm/μsec, Kramers' and atomic line radiation become the predominant source of radiation. They will comprise the major heating fluxes in the blunt body flight regime where radiative heating is the dominant heating flux. As there appears to be some controversy as to the proper Kramers' radiation calculation for nonhydrogen-like atoms, a brief survey of the calculations available for this source of radiation from an equilibrium gas sample is given. A proper criterion for selection between the various Kramers' calculations should be the comparison of these calculations with data.

Kramers' radiation comprises both the radiation produced by the deceleration of an electron in the electric field of an ion or atom (called free-free) and the capture of an electron by an ion (called free-bound). For hydrogen, one may calculate the free-bound absorption coefficient for an optically thin gas sample from:[20]

$$\sigma(\nu, n) = \frac{32\pi^2 e^6 R Z^4 N_e N_i \nu^3}{3\sqrt{3}\,(2\pi mkt)^{3/2} n^3 c^3} \; e^{\frac{hc\nu}{kT}} \qquad (1)$$

where ν is expressed in cm^{-1}, e is the charge of the electron, R is the Rydberg constant, Z is the charge of the nucleus, N_e and N_i are the particle concentrations of the electron and ion, respectively, m is the mass of the electron, n is the principal quantum number of the initial

state, and T is the temperature in degrees Kelvin. The calculation for the total absorption coefficient is then carried out by summing over all states with the same principal quantum number, n , and then integrating over the energy levels of the free electrons. The relationship between the absorption coefficient and the emissivity of a gas is then given by Kirchoff's Law.

Unsöld[21] extends this expression, which was derived for hydrogen atoms, to more complex atoms. The structural peculiarities of complex atoms were taken into account by introducing an effective nuclear charge, Z_{eff}, and a factor, γ , which is the ratio of the number of sublevels of a complex atom with a given n and ℓ to an analogous quantity for hydrogen, where ℓ represents the orbital angular momentum quantum numbers.

The energy of a state for a given n and ℓ is then:

$$E_{n\ell} = -\frac{R Z_{eff}^{2}}{n^{2}} \tag{2}$$

Because of the more uniform distribution of energy levels in the case of complex atoms, it was possible to extend the integration over all the excited states. As a result, an expression for the free-bound radiation per unit volume per steradian per wave number in cm^{-1} can be obtained. For $\nu \leq \nu_c$:

$$\mathcal{E}_{\nu fb} = \frac{16\pi^{1/2} e^{6} N_e N_i}{3\sqrt{6}\, m^{3/2} c^{2} (kT)^{1/2}} \left(Z_{fb}^{2} - Z_{ff}^{2} e^{\frac{-hc\nu}{kT}} \right) = \tag{3}$$

$$1.63 \times 10^{-35} T^{-1/2} N_e N_i \left(Z_{fb}^{2} - Z_{ff}^{2} e^{-hc\nu/kT} \right) \frac{w}{cm^{2}\ ster}$$

and for $\nu \geq \nu_c$:

$$\mathcal{E}_{\nu\,fb} = 1.63 \times 10^{-35} T^{-1/2} N_e N_i \left(Z^2_{fb} e^{-hc(\nu - \nu_c)/kT} - Z^2_{ff} e^{-hc\nu/kT}\right) \tag{4}$$

ν_c is the limiting frequency up to which the energy levels can be regarded as being continuous, and Z_{fb} and Z_{ff} are the effective nuclear charges for free-bound radiation and free-free radiation, respectively.

The free-free contribution is given by:

$$\mathcal{E}_{\nu\,ff} = 1.63 \times 10^{-35} T^{-1/2} N_e N_i Z^2_{ff} e^{-hc\nu/kT} \tag{5}$$

for $\nu \leq \nu_c$ and for $Z_{ff} = Z_{fb}$, the total continuum radiation according to expressions (3) and (5) is:

$$\mathcal{E}_{\nu}\ \text{total} = 1.63 \times 10^{-35} T^{-1/2} N_e N_i Z^2 \tag{6}$$

Lindenmier[22] developed a calculation for the total Kramers' radiation which attempted to take into account the fine structure of the free-bound radiation at shorter wavelengths. Z^2_{fb} and Z^2_{ff} were both estimated to be 1.4 from the best straight line fit through an $E_{n\ell}$ versus $1/n^2$ curve, Eq. (2). Instead of using an expression similar to Eq. (1) to obtain the detailed structure at the shorter wavelengths, the capture of electrons by various levels of the nitrogen ion was related to the corresponding continuum oscillator strengths of hydrogen for the same n and ℓ

values. The use of the hydrogen oscillator strengths for nitrogen is probably not justifiable.

Biberman and Norman[23, 24] have obtained corrections to the Unsöld-Kramers' formula for radiative recombination using the quantum defect method of Burgess and Seaton.[25] They calculate a quantity $\xi_{(\nu, T)}$ which is a correction factor for Eq. (3) with $Z_{fb} = 1$. The total continuum radiation becomes

$$\mathcal{E}_{\nu} = 1.63 \times 10^{-35} T^{-1/2} N_e N_i \left[\xi_{(\nu, T)} + \left(Z^2_{ff} - \xi_{(\nu, T)} \right) e^{-hc\nu/kT} \right] \quad (7)$$

The quantity $\xi_{(\nu, T)}$ takes into account the capture of the electron to various levels of the nitrogen atom, and averages over the various electron levels so that the free-bound emission edge structure is lost. However, the calculation is not subject to the assumption that the electronic levels of nitrogen and hydrogen have the same continuum oscillator strengths.

B. Atomic Line Radiation

Calculations of atomic line radiation for spontaneous emission for an optically thin gas at thermodynamic equilibrium are relatively easy once the Einstein coefficient for a particular transition, the species concentration, the deactivation cross-section for the emitting state, and the temperature are known. The Einstein coefficient, A_{nm} is equal to $1/t_R$, where t_R is the radiative lifetime for the particular transition and is related to the f number oscillator strength for that transition.

The intensity of radiation of a given line per steradian per unit volume is given by the relation

$$I = \frac{hc\nu \; N_n \, A_{nm}}{4\pi (1 + t_c \, A_{nm})} \tag{8}$$

where N_n is the particle density of excited atoms. The factor 1 $(1 + t_c \, A_{nm})$ includes the effect of collision limiting,[7] where t_c is the collision time for deactivation of the excited state. This factor will also apply to collision limiting of molecular radiators. A good deal of theoretical and experimental work has been done regarding the atomic line oscillator strengths for the constituents of air; namely, nitrogen and oxygen.[26, 27] However, the measurements and calculations of atomic line oscillator strengths are confined to the wavelength region below 1.2μ.

Self-absorption is one effect which will limit line radiation since the radiancy for a given line from a gas in thermodynamic equilibrium cannot exceed that of black body. Under these conditions, the line width determines the amount of energy which will escape from the gas. Stark and Doppler broadening are the two mechanism which will be important for determining the line width under the conditions for high speed shocks at low densities. At high enough pressures, pressure broadening will be dominant. The natural line width can be neglected relative to these types of broadening.

C. Comparison of Calculations with Data

The above Kramers' and atomic line radiation calculations are the basis for the comparison of equilibrium data with theory in the present

investigation.

Figure 12 presents calculations for the various equilibrium contributors which should be important for the 10 mm/μsec air shock at initial pressure 0.1 mm Hg. The Biberman "total" line is the sum of the Biberman free-bound calculation, plus the free-free calculation of Eq. (6) based on a $Z^2_{ff} = 1$. The calculation of Biberman and Norman for the free-bound Kramers' radiation for N^+ and O^+ is preferred because it has a firmer theoretical basis than that of Lindenmier's. The calculation for the O_{fb} is based on the photoabsorption measurements of Branscomb, et al.[30] An effective Z^2 of 0.1 is used for the Kramers' radiation due to the scattering of electrons by neutral nitrogen atoms as determined by Taylor.[31] The $N_2^+(1-)$ calculation for these shock conditions is based on the f number of .035 as evaluated by Keck, et al.[8] The $N_2(2+)$ calculation is based on the f number of .09 published in Ref.10. The calculation for the intensity of the nitrogen atom lines at 0.87 and 1.0μ with 0.02μ resolution were based on the Einstein coefficients published by J. Richter[26] and do not include the effect of collision limiting. At these wavelengths, the lines are essentially optically thin, since the brightest peak intensity of any of the lines does not exceed 10% of the black body based on their Doppler widths.

Comparison between these calculations and the data is made in Fig. 4 in which the Biberman and Norman total radiation calculation, excluding atomic line radiation, is shown. Referring also to Fig. 12, one concludes that the Biberman and Norman method is the best calculation for obtaining the level of the intensity of Kramers' radiation. This is also expected on

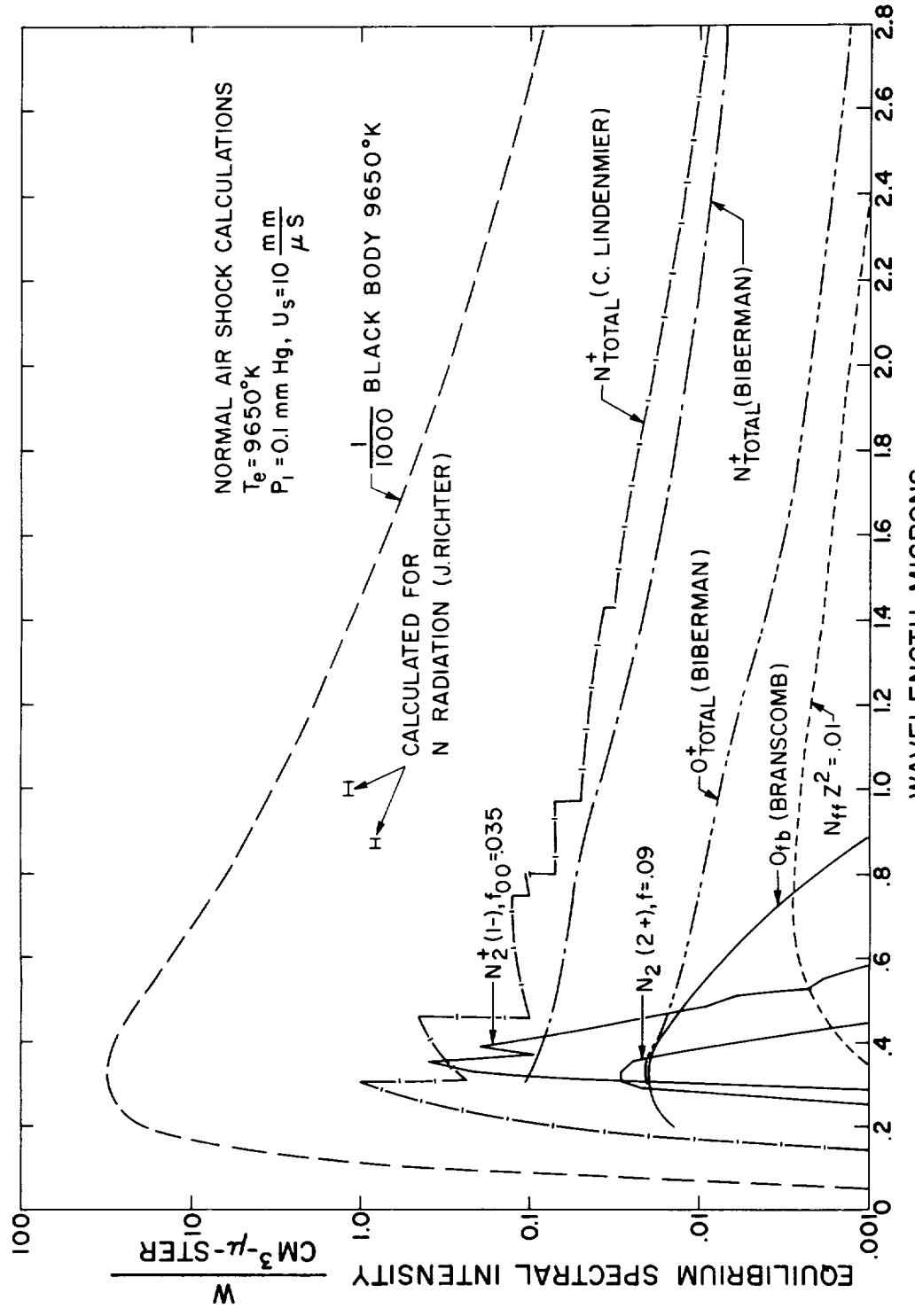

Fig. 12 Calculations of the important radiation which should be the major constitutents of the equilibrium radiation behind incident air shocks, U_s = 10 mm/μ sec, P_1 = 0.1 mm Hg.

a theoretical basis and is in accord with a comparison of a N_{fb} Biberman calculation with arc measurements reported by Boldt.[32, 33]

The photoemission edges due to the capture of electrons by various levels of the atom should be present, and the Lindenmier calculation will give the proper wavelength location of these edges, although not with the right intensity. It is possible that these edges are the main contributors to the radiation measurements at .25 and .29μ in Fig. 4 since there should be no molecular radiators contributing at these wavelengths under these shock conditions.

The radiation between .8 and 1.5μ is attributed mainly to atomic N and O line radiation. Calculations of N line radiation contributors at .87μ and 1.0μ in Fig. 12 agree well with measurements. These calculations were made assuming no self-absorption of the lines. This assumption is reasonable since the Doppler width of these lines is wide enough so that under the conditions of the measurements none of the line centers would exceed 10% of the black body. This assumption was also experimentally justified by doubling the optical path. This doubled the output signal in the region of the lines which is to be expected for thin gas radiation. At wavelengths longer than 1.1μ, the oscillator strength for bound-bound transitions of nitrogen and oxygen atoms were not available and, hence, no calculations for the line radiation have been made in this region.

Calculations for the velocity and density dependent equilibrium radiation data were shown in Fig. 5. The important molecular radiation contributors in the indicated wavelength intervals; namely, $N_2^+(1-)$ and

$N_2(2+)$ were calculated according to the methods outlined by Keck, et al in Ref. 8. The calculations in Fig. 5 (a) and (b) for the $N_2^+(1-)$ at 1.0 mm Hg, P_1, and in the velocity range 5 to 8 mm/μsec agree well with the expected values. However, at higher velocities, and at 0.1 mm Hg, P_1, more radiation is seen than predicted. The calculation of the $N_2^+(1-)$ radiation assumes an f number at the 0, 0 transition of .035 with no matrix element dependence on internuclear separation. The recent Keck, et al[8] review of previous shock tube results supported by other methods for obtaining molecular electronic transition moments indicates that the f number of .035 for the $N_2^+(1-)$ system at the 0, 0 transition is probably correct to within a factor of 2.

A possible contribution to the excess radiation of the higher velocity and lower density measurements of Fig. 5 (a) and (b) are the photoemission edges produced by the capture of free electrons to various electronic levels of either nitrogen or oxygen ions. Another possibility, and the one which is more likely, is that the excess radiation is produced by CN. Since CN is isoelectronic with N_2^+, the CN violet system would look identical to that of $N_2^+(1-)$ when viewed with coarse resolution. The measurements of 5 (c) agree well with the calculations of N atomic line radiation based on the Einstein coefficients published by J. Richter[26] and do not include self-absorption or collision limiting effects.

In conclusion, the important features of the equilibrium radiation behind strong incident air shocks in the wavelength interval from .25 to 2.0μ are : (1) molecular band radiation contributes increasingly less and less to the radiation as the velocity increases about 9 mm/μsec; (2) above

the velocities of approximately 9 mm/μsec, the atomic line and Kramers' radiation become the important radiators, with the atomic line radiation being the important feature from 0.6μ to 1.1μ and possibly extending farther into the infrared; (3) if one assumes that the radiation comprising the continuum as measured by the monochromator measurements is due to Kramers' radiation, then one must conclude that the calculations of Biberman and Norman give the most satisfactory fit to the data.

VI. NONEQUILIBRIUM RADIATION CALCULATION

A. Present State of Theoretical Knowledge

Two steps toward understanding nonequilibrium radiation for a normal shock front are a knowledge of the chemical kinetics of high temperature air, and also an understanding of the contributions of molecular, atomic and Kramers' radiation to the luminous front region. A prediction of radiation must rely on calculations of the temperature, density and particle concentration histories behind the shock front from a density model, as well as a knowledge of the excitation mechanism for each radiating species.

Calculations of the thermodynamic conditions can be made by integration of the chemical and ionization rate equations with a given set of rate constants. The relevant chemical rate constants are reasonably well known[34] for temperatures up to 8,000°K. However, to make calculations for shock speeds of 40,000 ft/sec, it is necessary to extrapolate the assumed temperature dependence for these rate constants to temperatures of 75,000°K in some cases. In this higher temperature regime, ionization becomes energetically more important than it was where energy primarily goes into dissociation. Ionization rates are known for shock velocities below 9 mm/μsec. In the higher flight speed regime, they become important for describing both the thermodynamic history and radiation history in the relaxation region.

In addition to the uncertainty in the ionization process, the coupling between the various relaxation processes is not completely understood;

determination of some of the pertinent chemical rates were made by examining the rate of decay of the radiative relaxation profiles very near the equilibrium region.[35] The rates were chosen to fit the radiation profiles in the region near equilibrium, where the molecular vibration and electronic degrees of freedom have relaxed over a wide range of conditions. Hammerling, et al[36] proposed a coupling of vibrational relaxation with the dissociation process which stated that dissociation can take place equally well from any vibrational level in the ground state molecule. The over-all effect of this coupling was to slow down the dissociation rates in the gas until vibration had relaxed to the local translational temperature. At this time, the dissociation rates can proceed at their full values. When the chemical rates are extrapolated in the usual manner and the coupling scheme of Ref. 36 is used, good agreement is obtained between experiment and theory in the radiative relaxation region near equilibrium.[35] This process has been carried out in air and it has been demonstrated that the calculations of translational temperature, density and particle concentrations are approximately correct.

More recently, Treanor, et al[37] have examined theoretically the coupling between vibration and dissociation behind strong shock waves and show that the loss of vibrational energy during dissociation introduces an inverse temperature dependence into observed dissociation rates. They further showed that a dissociation-incubation time results if Hammerling's model is changed so that dissociation from higher vibrational levels is enhanced. Wray[38] has demonstrated experimentally

that this incubation time does exist for the dissociation of oxygen. This modification to the calculation of particle and density concentration behind shocks can be carried out. Despite the extreme extrapolation necessary and the unknowns discussed above, chemistry does not appear to be the main problem in our effort to synthesize the radiative mechanisms of the shock front.

Understanding the luminous front radiation hinges upon a knowledge of how energy initially invested in heavy molecules is transferred to molecular and atomic electrons and to ionization. A small amount of progress has been made in understanding molecular excitation in the shock front. A tentative hypothesis has been made that molecular electronic degrees of freedom are strongly coupled to vibrational energy in the gas.[35] This hypothesis is in accord with observations in gas discharges where radiation is quenched more effectively by molecules than by atomic collisions.[39] It is also in accord with temperature measurements in nitrogen shocks made by F.S. Faizullov, et al[40] using sodium line reversal techniques. He observed that the population of excited sodium atoms followed the vibrational temperature of the nitrogen. There are other indications, notably the work of Gaydon and his co-workers,[41, 42] that such a coupling exists. With a different approach in mind, Wray has been performing experiments in $N\text{-}N_2$ mixtures and has found that the N atom is a good catalyst in exciting the $N_2(1+)$ system at the shock front. These findings regarding excitation mechanisms are a beginning; however, as yet, no satisfactory theory has been developed by which nonequilibrium molecular radiation can be calculated. This present study has further indicated that

atomic lines as well as molecular systems can overshoot in the relaxation region further complicating the theoretical picture.

There is experimental indication that as one goes to a high enough velocity at a given initial pressure, the luminous front overshoot disappears. This can be seen qualitatively by comparing the nonequilibrium data of Fig. 9 with that of the equilibrium data of Fig. 5. The equilibrium data at the higher velocities is more velocity-dependent than the non-equilibrium radiation. At a given wavelength and initial pressure, a shock velocity is found where the equilibrium radiation level is comparable to the peak nonequilibrium radiation. Qualitatively, the velocity where this occurs increases with decreasing initial pressure. The significance of this finding is that it somewhat simplifies gas cap radiation calculations for high flight velocities since, for practical purposes, it reduces to an equilibrium solution.

B. Summary of Nonequilibrium Radiation Data

A summary of the present data and that of Ref. 5 on total nonequilibrium radiation is shown in Fig. 13. The 33,000 ft/sec data point refers to the 40 watts/cm^2 -2 π evaluated from Fig. 6. This value is possibly high by as much as a factor of two. Since no adequate nonequilibrium radiation theory is available, any value of total nonequilibrium radiative heating which is inferred from measurements of limited wavelength coverage must be treated with skepticism. Therefore, the dashed line in Fig. 6 was drawn purposely generous in the wavelength regions where no measurements are available. The value of 40 watts/cm^2 - 2 π, at 33,000 ft/sec can thus be considered a reasonably good upper limit but should not be regarded as a definitive value.

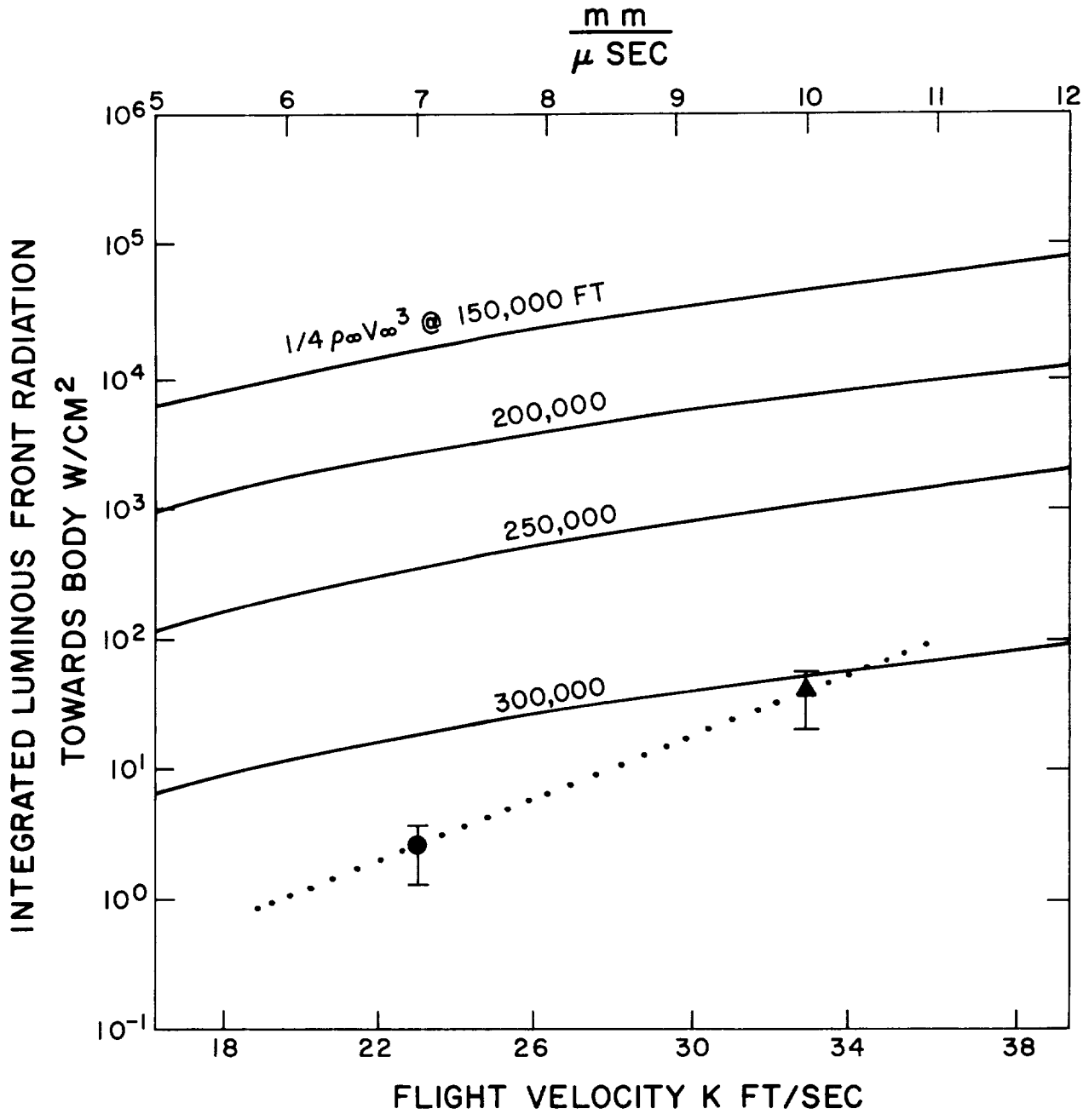

Fig. 13 A summary of existing Avco-Everett Research Laboratory nonequilibrium radiation data in terms of total radiation emitted from one side of an infinite slab corresponding to a shock front of infinite extent. The two data points at 23,000 and 33,000 ft/sec are based on detailed wavelength studies of limited spectral coverage.

The data point at 25,000 ft/sec was presented in Fig. 5 and is subject to the same criticism as the 33,000 ft/sec value. The proper values probably fall within the ranges indicated by the brackets around the two points.

Flow energy curves have also been plotted in this figure for comparison with the nonequilibrium radiation. Since the radiation is in terms of the radiation per 2π steradians, 1/2 the flow energy, the value $1/4\ \rho_\infty V_\infty^3$, is plotted. For velocities less than escape velocity and at altitudes below 250,000 ft, the nonequilibrium radiation never represents more than 10% of the flow energy and should have very little effect on the over-all energy balance.

VII. NONEQUILIBRIUM AND EQUILIBRIUM RADIATION IN FLIGHT

A. Empirical Calculation Scheme

As our understanding of the mechanism whereby the excited radiating states are produced is incomplete, we are not in a position to calculate the nonequilibrium radiation time history for a shock front from a theoretical model. Estimates of the nonequilibrium radiation widely differing from reality have resulted from this lack of knowledge of the excitation mechanism and its rate.[9] In lieu of a complete theory of the nonequilibrium shock front radiation based on the experimental data, a semiempirical calculation scheme which approximately reproduces the observations must suffice. The measured radiation rise times are the basis of the proposed calculation scheme.

The variation of the thermodynamic properties and species concentrations behind a shock front can be calculated[36] due to the effects of nonequilibrium chemistry. A decay in radiation for such a shock front can be calculated by assuming that the translational temperature is the appropriate temperature governing the population of the excited levels of the radiating molecules. The contributions from the various species, particularly the three dominant nitrogen molecular band systems N_2^+, $N_2(1+)$ and $N_2(2+)$ can be formulated from a knowledge of the f numbers as outlined by Kivel and Bailey.[6] The accuracy of these tables is not the subject of lengthy discussion here. These tables need to be modified in several ways. The f numbers for several of the molecular radiators in these tables need modification.[13, 43]

A reconsideration of Kramers' radiation and atomic line radiation, the latter of which is not included in the tables, is also required. The present status of knowledge of air molecular radiators is discussed in Ref. 8, while the status of Kramers' and line radiation is touched on in a previous section of this study.

The radiation profile calculated for a normal shock of 9.64 mm/μsec (31,600 ft/sec) is shown in Fig. 14. The rise time of the radiation was taken from the data of Fig. 10 properly scaled for binary chemistry. An experimental profile of the radiation observed in the wavelength region between 0.55 and 1.0μ is compared to the calculated one. As the time to peak is normalized in the calculation, this agreement is not surprising. However, the absolute magnitudes are not normalized. The high equilibrium level reached by the measurements is due to sources of other than the nitrogen band systems which were not included in the calculation scheme, namely Kramers' radiation and atomic lines. If the nonequilibrium radiation is predominantly due to the molecular bands of nitrogen, the overshoot should initially correlate with the radiation calculated considering the nitrogen bands only and, at later times, it should approach an equilibrium value which includes the contributions from all sources. This general characteristic is seen in the correlation between the radiation measurement and the calculation scheme. The total radiation profile is thus obtained by fairing the molecular band system contributions during the nonequilibrium front into the equilibrium levels. A better calculation scheme than this empirically correct description of the details of the shock front is probably beyond our present knowledge.

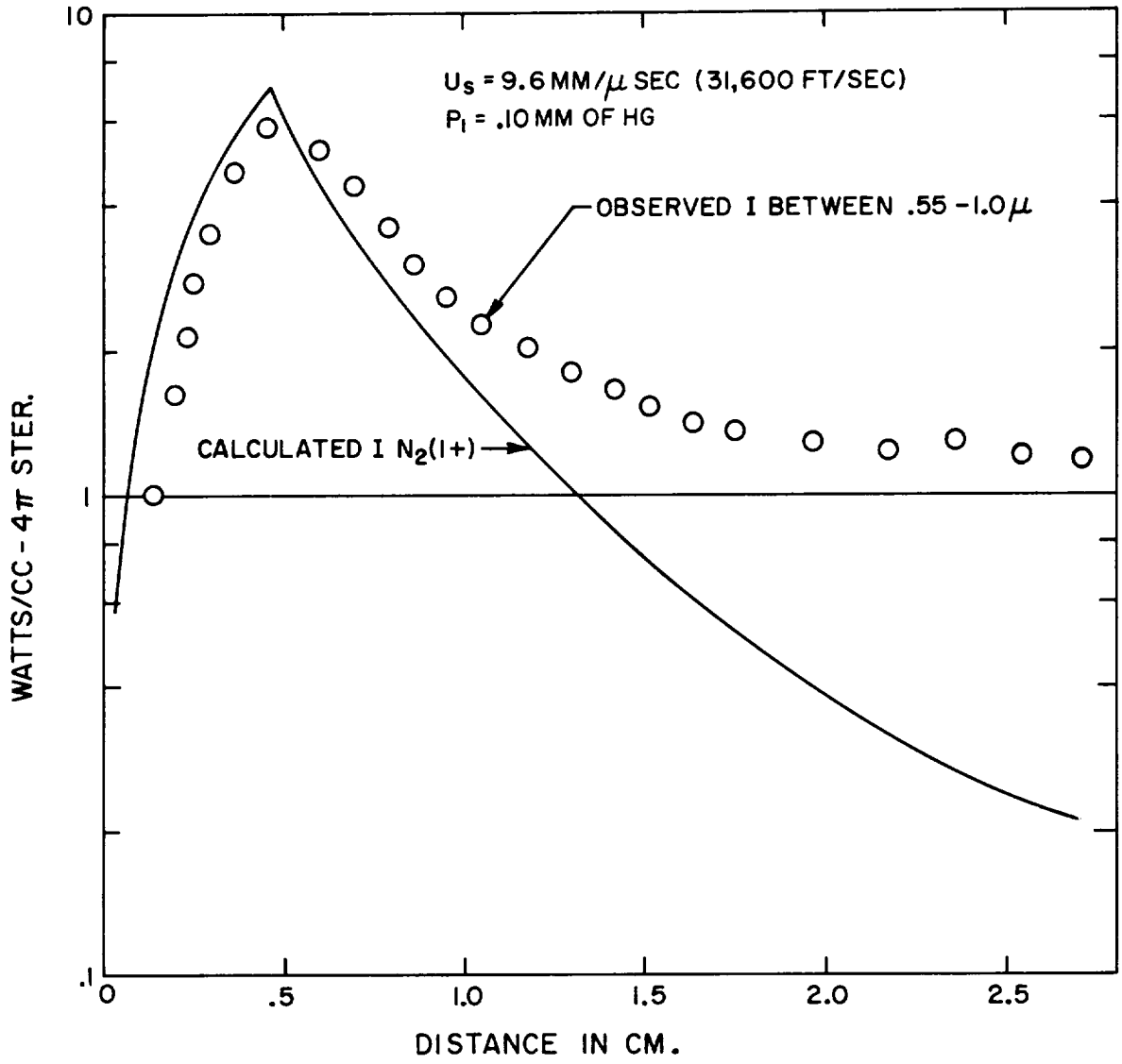

Fig. 14 Calculated profile of nitrogen molecule, first positive band system radiation, and the measured profile in the wavelength interval from .55 to 1.0μ. The experimental profile is postulated to be produced by the overshoot of the N_2(1+) radiation followed by the decay to the total equilibrium value which in this wavelength region should have strong contributions due to Kramers' radiation and atomic nitrogen lines. The fairing of the N_2(1+) overshoot into the total radiation is the model used in these calculations.

The value for the integrated nonequilibrium radiation calculated in this fashion was found to be very sensitive to the distance to the radiation peak. If the distance to the radiation peak was small enough, a significantly large energy loss due to radiation resulted in the calculation. It was necessary to include this energy loss in the conservation equations controlling the chemistry.

The predictions of this calculation scheme were compared to both the absolute value and velocity dependence of the measured nitrogen, first, and second, positive band system radiation in Fig. 9 (A, D). The agreement of the $N_2(1+)$ band system, i.e., Fig. 13 (D), is quite good in the velocity range investigated. The less satisfactory agreement for the $N_2(2+)$ data, i.e., Fig. 9 (A), at velocities above 8 mm/μsec is not too surprising in view of the crudeness of the calculation scheme.

B. Flow Field Calculations

The function of the empirical calculation scheme for nonequilibrium radiation is to allow an estimation of the three dimensional effects for a shock standing in front of a blunt body. It would be highly desirable to treat the blunt body problem simply as a normal shock or as some simple modification, thereof. However, as a streamline very near the stagnation point travels along the body for distances which are of the order of ten times the stand-off distance of the shock at the stagnation point, it is dangerous to assume a priori that the normal shock properties can be correlated to the blunt body situation.

Several methods have been developed to introduce finite rate chemistry into flow field calculations. The computational difficulties of this

method are considerable and although attempts are being made in this direction, only the two limiting cases, equilibrium and frozen characteristic calculations, are available both for the subsonic and supersonic portions of the flow field.[44, 45]

In lieu of a complete nonequilibrium solution, several investigators have combined normal shock wave chemistry calculation programs with a streamtube method for calculating a flow field. In this method, a pressure history is prescribed from either equilibrium characteristics, frozen characteristics, blast wave theory, or any other assumption into which the products of the normal shock calculation are forced to flow. The locations of the streamtubes can be determined from conservation of mass.

Another approach to the subsonic portion of the blunt body program is the inverse method of the flow field calculation.[46] In this method, a body shape is found by stepwise integration of the conservation laws starting with a known shock geometry. Marrone[47] has added the rate equations for the important reactions to high temperature air to this procedure, and thus can calculate a nonequilibrium flow field by the inverse method. An a priori knowledge of the shock wave shape which results in a given body geometry is required by this method.

The inverse method has the advantage of accounting for modifications of the bow shock due to nonequilibrium effects. A change by about a factor of two occurs in the shock detachment distance between equilibrium and completely frozen flow. However, this effect will only be present at very high altitudes where the flow is strongly frozen. The assumption of

continuum aerodynamics is questionable under these conditions. When the flow is a mixture of nonequilibrium and equilibrium flow, the modification of the shock position due to nonequilibrium effects is very small and, consequently, the simpler streamtube method is equally applicable.

For blunt bodies, the pressure distribution on the forward face is not affected by the chemistry. Consequently, a modified Newtonian assumption is satisfactory for describing the pressure distribution along the shock front, and on the body surface for the forward face. Once the pressures on the shock and the body surface have been specified, streamlines can be located by judicious use of the conservation laws, radial pressure gradients, and assuming the flow is in thermodynamic equilibrium. From streamline locations thus constructed, the pressure history along the streamlines can be determined. Using these pressure histories in terms of distance behind the shock front as an input, the shock front chemistry calculation can be performed. Different normal shock strengths identify the streamlines, i.e., the shock strengths representative of the location along the bow shock wave where the streamline intersects the shock. This calculation procedure gives the nonequilibrium flow parameters along each streamline.

We assume differences in streamline locations between the equilibrium and nonequilibrium flow. Although this is a reasonable assumption, the shock front and streamtube positions could be recalculated after the nonequilibrium mass flow parameters have been determined by an iterative procedure to remove this restriction.

C. Normal Shock Radiation Calculation Scheme and Flow Field

The radiation field appropriate to the above calculated nonequilibrium conditions along streamlines can be calculated by applying the normal shock procedure previously described. Because of the pressure gradients present along streamlines and the subsequent acceleration of the flow, the radiation history must be calculated by determining the excitation process in particle time. The implicit assumption is that the particle times to peak radiation, as well as throughout the nonequilibrium region, are invariant between the normal shock and blunt body streamline cases, despite the pressure gradient differences.

Calculations have been carried out for a two-foot radius sphere flying at 35,000 ft/sec at an altitude of 200,000 ft (1959 ARDC Atmosphere).[48] The radiation intensity is first obtained in terms of the coordinate along streamlines. It has been found useful to present the results in terms of radiation along annular cuts taken through the flow field at various radial distances from the center line, as shown in Fig. 15. The nonequilibrium effects are seen to be restricted to a rather narrow region. Consequently, as an integrated effect, equilibrium radiation dominates for the case shown. The integrated nonequilibrium radiation is only about one-third of the total radiation seen by the body in the strong shock portion of the stagnation region. Scaling the results to a one-foot nose radius body at the same speed and altitude, the nonequilibrium contribution would be approximately half the total radiation.

The radiation intensity resulting from integrating under the profiles shown in Fig. 15 are shown in Fig. 16. The relative intensities due to

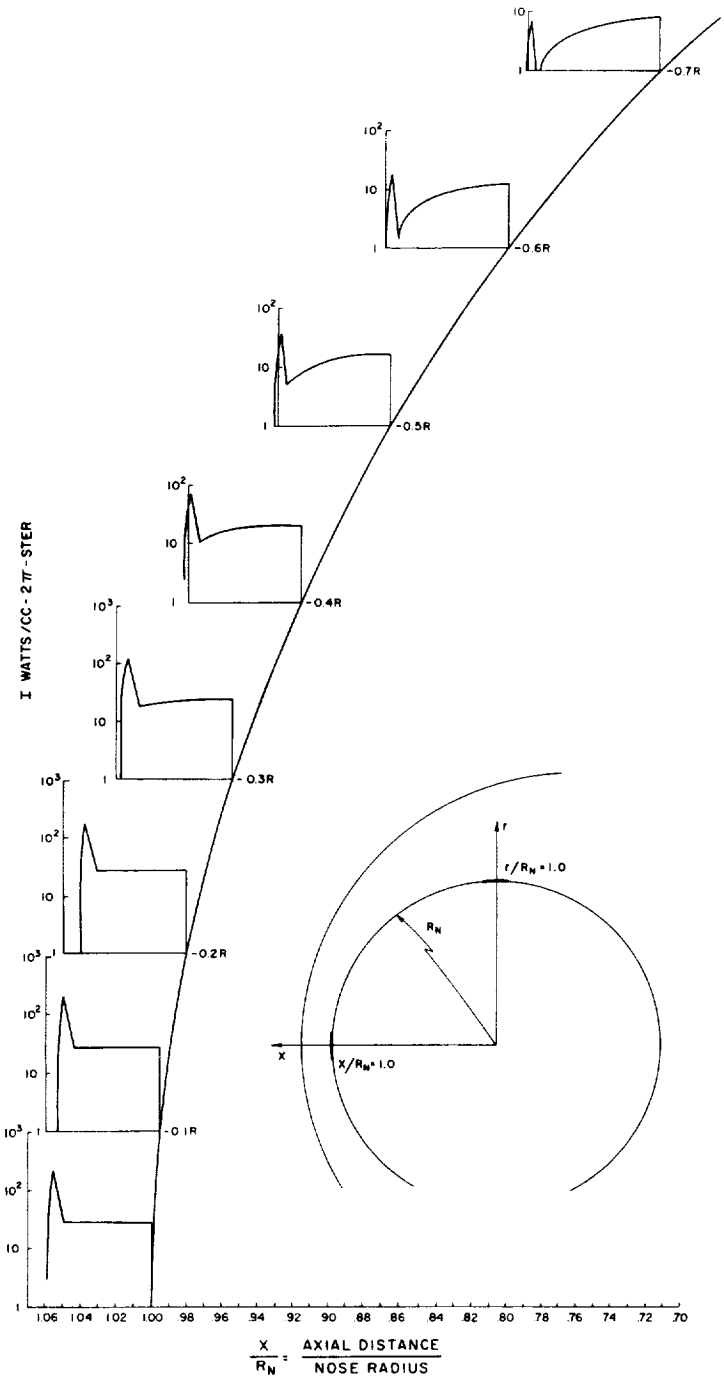

Fig. 15 Radiation profiles along annular cuts through the inviscid flow around a spherical nose body with a two-foot radius, flying at a 200,000-foot altitude. Note that for the inner radii, the normal shock is a very good approximation, while at the outer radii, the isentropically expanded stagnation region air gives considerably more radiation than the gas at the shock at the same radius.

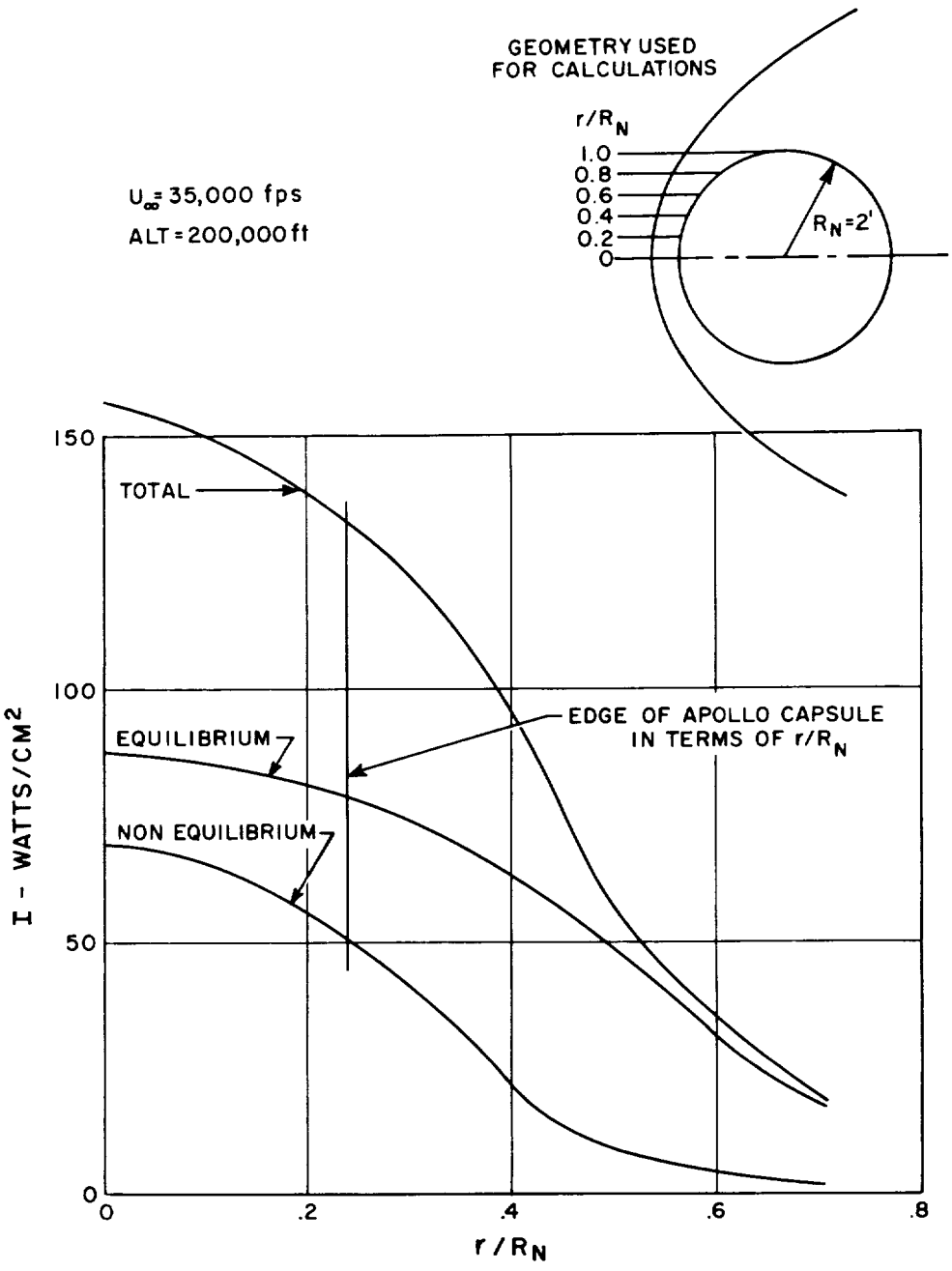

Fig. 16 Distribution of equilibrium, nonequilibrium and total radiation for a two-foot nose radius sphere flying at a 200, 000-foot altitude at 35, 000 ft/sec. This is the distribution available in the flow which is not quite the same as the distribution seen by the body surface.

equilibrium and nonequilibrium radiation are shown, as well as the total of the two contributions. The integrated radiation seen by the nose of a spherical body can be approximated quite closely by the normal shock value out to annulii of radius ratio, r/R_n, of at least 0.2 if not out to 0.3. This region includes angles of about 15^o to the flight velocity vector. Outside this central region, both equilibrium and nonequilibrium radiation drop rather rapidly and can in many cases be ignored completely. It is interesting to note that although in streamline coordinates the nonequilibrium zone gets considerably wider for the outer streamlines, the thicknesses of the profiles at various annulii do not vary greatly. The closer spacing of the streamtubes in the vicinity of the shock corresponding to the increase in flow per unit area with increasing distance from the body in a direction normal to the surface gives this result.

The integration along annular cuts shown in Fig. 16 gives the radiation field surrounding the body. The quantity of actual interest is the radiation incident on a given point of the body surface. At each point, an integration must be performed over all angles to determine what fraction of the radiation shown in Fig. 15 falls upon that point on the body surface. The result of this inversion of the radiation data is shown in Fig. 17 along with the total radiation curve from Fig. 16 Even at the stagnation point, the radiation falling on the body is slightly less than the radiation field value. In an axisymmetric body problem, the radiation always falls off axis and, thus, the intensity seen by any point on the body is lower than the value in the flow field at that point.

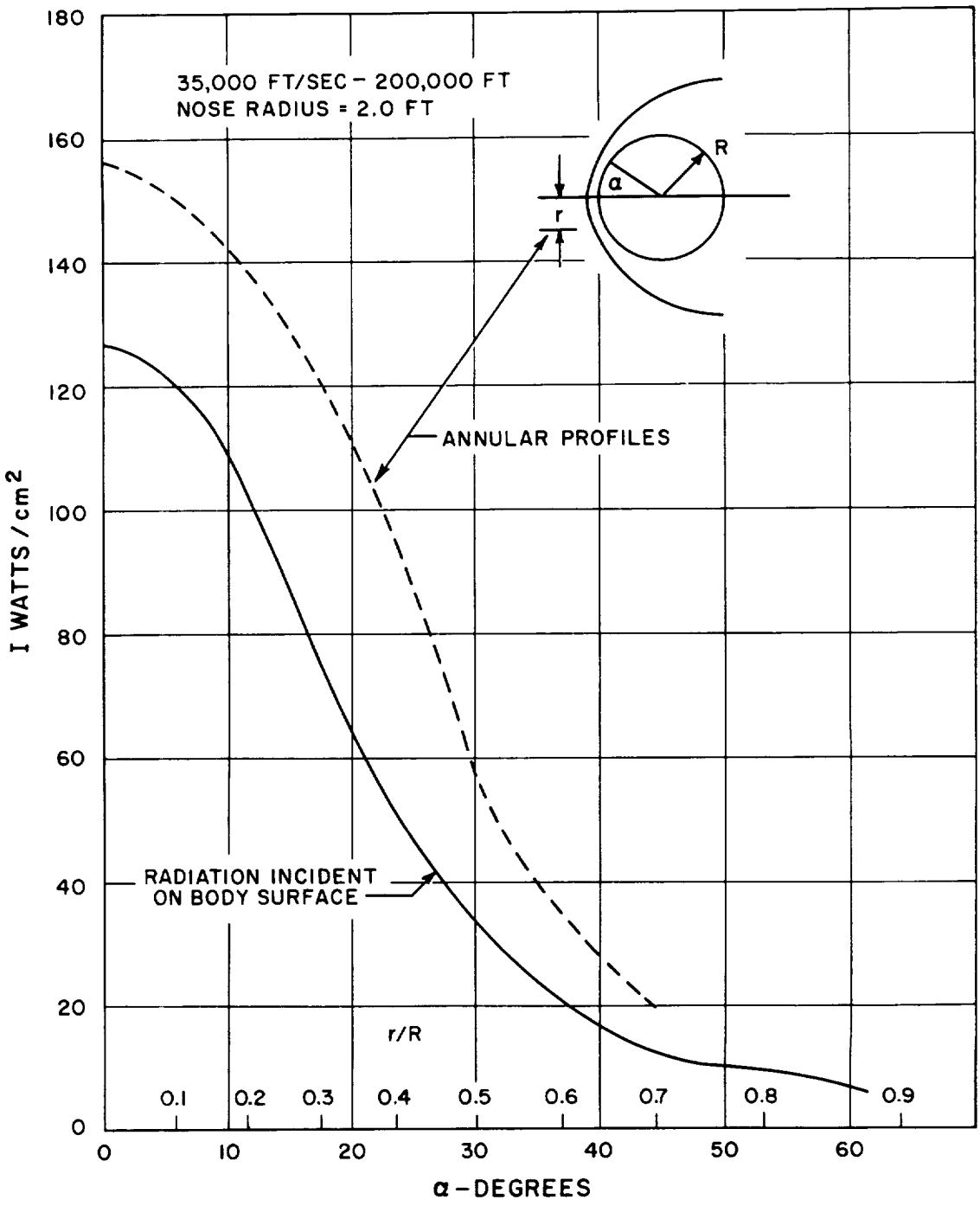

Fig. 17 Comparison between radiation integrated over annular profiles and radiation as seen by various points on the body surface.

For the outer annulii, the strongest radiation emanates from the regions close to the body and, consequently, from the gas along the streamlines which crossed the strong shock near the stagnation point. Excluding viscous and nonadiabatic effects, the radiation intensity along these streamlines maintains an intensity of about one-third its normal shock value out to an annulus ratio of 0.7. The radiation behind the oblique shock at this radius ratio has fallen by as much as two orders of magnitude from the stagnation point value. This is, of course, due to the differences in the entropy of the two streamlines. The stagnation streamline having gone through a very strong shock has considerably higher entropy than an outer streamline, say the one intersecting the shock at $r/R = 0.625$ where the component of velocity normal to the shock is only 80% of U_∞. Under the Newtonian assumption, both streamlines have approximately the same pressure at the same radius ratio annulus, differing only by the effect of radial pressure gradient. The result is that the high entropy stagnation streamline air is considerably hotter than the lower entropy outer streamline directly behind the shock. As a consequence of this phenomenon, the radiative heat transfer does not show the rapid decrease with radius ratio, r/R_n, which would be predicted without considering streamtube flows. The equilibrium radiation distribution shown in Fig. 17 is considerably flatter than the distribution calculated by Wick.[49]

The above distribution may become less flat at very high velocities and altitudes because the stagnation streamline will be the first to be effected by viscous and nonadiabatic effects. The first of the two above

effects has not been considered. The latter has been accounted for in the chemistry program by including a radiation loss term in the energy balance along a streamline. For the example chosen, the energy loss at the stagnation point amounts to 1.60% of the incident kinetic energy. The total energy loss including the outer annulus ratio is, of course, much smaller due to the decrease in radiation with r/R_n.

The sphere calculations presented above can be scaled to other geometries by using appropriate scaling laws.[5, 50] The nonequilibrium shock front behaves like a binary phenomenon. The equilibrium region can be scaled according to the tables of Ref. 6. Thus, with some judicious assumptions, the single calculation shown can be used to construct complete trajectory histories. Further refinement of this calculation is probably not warranted at the present time because of the many uncertainties about the basic radiation phenomena which have been pointed out earlier in this paper.

VIII. SUMMARY

Investigations performed in connection with an experimental and theoretical study of the equilibrium and nonequilibrium radiation from high temperature air under the conditions encountered by a super-satellite re-entry vehicle have been discussed. The radiation from normal shock waves of over 40,000 ft/sec has been observed. These shock waves were produced in an electric arc driven shock tube.

Most of the measurements reported were made by calibrated monochromators and photomultipliers. Some data was achieved by photoelectric gauges, infrared detectors, and photographic techniques. Although the wavelength coverage was limited in some regions, an absolute spectral distribution of the nonequilibrium radiation was synthesized by repeated measurements with a narrow band width. Integration of the spectral distribution has allowed us to estimate an upper limit for the total nonequilibrium radiative heat flux.

Absolute equilibrium radiation data were also collected. New data on Kramers' radiation indicate this source to be less intense than previous estimates. However, atomic line radiation was observed which previously had not been seen in laboratory experiments. These two observations leave unanswered many questions about radiation from air at temperatures of 10,000°K and above. The greatest unknown in a theory of nonequilibrium radiation from air appears to be the excitation mechanism whereby the energy originally in the heavy particles is transferred to the electronic states and ionization. Experiments have been

performed which allow a semiempirical calculation procedure of non-equilibrium radiation from a shock front. A streamtube method has been used to extend this procedure to the three dimensional blunt body flow problem.

The major questions which have been left unanswered regard the absolute magnitude of the equilibrium radiation due to Kramers' radiation and atomic lines. Several regions in the spectrum, such as the ultraviolet and the near infrared, should receive additional coverage to guarantee that no significant radiators are present at wavelengths not covered at present. The mechanisms by which excited electronic states and ions are produced also require much further study. Finally, the methods by which our knowledge of shock front radiation can be applied to the flow about bodies should be improved consistent with advances in the theoretical and empirical understanding of the radiation phenomenon.

ACKNOWLEDGMENT

The authors wish to give special credit to J. D. Teare who was mainly responsible for the flow field and radiation calculations, and to A. Textoris who helped perform the experiments.

The authors also wish to express appreciation for the many helpful suggestions given by J. C. Keck and to acknowledge the enthusiastic support given this work by A. R. Kantrowitz, Director of the Avco-Everett Research Laboratory.

REFERENCES

1. Fay, J.A. and Riddell, F.R., "Theory of stagnation point heat transfer in dissociated air," J. Aero. Sci., 25, 73-85 (1958).

2. Rose, P.H. and Stark, W.I., "Stagnation point heat transfer measurements in dissociated air," J. Aero. Sci., 25, 86-97 (1958).

3. Kivel, B., "Radiation from hot air and its effect on stagnation point heating," J. Aero. Sci., 28, 96-102 (1961).

4. Meyerott, R.E., "Radiation heat transfer to hypersonic vehicles," Lockheed Aircraft Corporation, Missile Systems Division, LMSD-2264-R1 (September 1958).

5. Camm, J.C., Kivel, B., Taylor, R.L. and Teare, J.D., "Absolute intensity of nonequilibrium radiation in air and stagnation heating at high altitudes," Avco-Everett Research Laboratory Research Report 93, December 1959; also, J.Q.S.R.T., 1, 53-75 (1961).

6. Kivel, B. and Bailey, K., "Tables of radiation from high temperature air," Avco-Everett Research Laboratory Research Report 121, December 1957.

7. Keck, J.C., Camm, J.C., Kivel, B. and Wentink, T., Jr. "Radiation from hot air, II," Avco-Everett Research Laboratory Research Report 42, February 1959; also, Annals of Physics, 7, 1-38 (1959).

8. Keck, J.C., Allen, R.A. and Taylor, R.L., "Electronic transition moments for air molecules," Avco-Everett Research Laboratory Research Report 149, April 1963.

9. Teare, J.D., Georgiev, S. and Allen, R.A., "Radiation from the nonequilibrium shock front," Avco-Everett Research Laboratory Research Report 112, October 1961; also, ARS Preprint 1979-61.

10. Kennet, H. and Strack, S.L., "Stagnation point radiative transfer," ARS Journal, 31, 370-372 (1961).

11. Lin, S.C., "A survey of shock tube research related to the aerophysics problem of hypersonic flight," ARS Reprint 1985-61.

12. Camm, J. and Rose, P.H., "Electric shock tube for high velocity simulation," Avco-Everett Research Laboratory Research Report 136, July 1962.

13. Allen, R.A., Camm, J.C. and Keck, J.C., "Radiation from hot nitrogen," Avco-Everett Research Laboratory Research Report 102, April 1961; also, J.Q.S.R.T., 1, 269-277 (1961).

14. Lin, S.C., Neal, R.A. and Fyfe, W.J., "Rate of ionization behind shock waves in air. I- Experimental results," Avco-Everett Research Laboratory Research Report 105, September 1960.

15. DeVos, J.C., "A new determination of the emissivity of tungsten ribbon," Physica, 20, 690-714 (1954).

16. Euler, J., "The graphite-carbon arc as a standard (source) of intense radiation," Sitzber Heidelberg, Akad, Wiss. Math - naturw. Kl. No.4, p.413 (1956-57).

17. Rose, P.H. and Nelson, W., "On the effect of attenuation of gas dynamic measurements made in shock tubes," Avco-Everett Research Laboratory Research Report 24, March 1958.

18. Camac, M., Camm, J., Keck, J.C. and Petty, C.C., "Radiation phenomena in air between 3000°K and 8000°K," Avco-Everett Research Laboratory Research Report 22, March 1958.

19. Hammerling, P., "Ionization effects of precursor radiation from shocks in air," Avco-Everett Research Laboratory Research Report 98, June 1960.

20. Handbuch der Physik, ed. S. Flugge (Springer-Verlag, Berlin, 1957), Vol.28 p.79-204.

21. Unsöld, A., "Continuous spectrum of high-pressure Hg lamp and similar gas discharges," Ann. der Physik, 33, 607-616 (1938).

22. Lindenmier, C.W., "Kramers' radiation from hot air," Avco-Everett Research Laboratory Research Note 157, September 1959.

23. Biberman, L.M. and Norman, G.E., "Calculations of photo-ionization absorption," Opt. i Spektr., 8, 433-438 (1960).

24. Biberman, L.M., Norman, G.E. and Ulyanoo, K.N., "On the calculation of photo-ionization absorption in atomic gases," Opt. i Spektr., 10, 565-569 (1961).

25. Burgess, A. and Seaton, M.J., "A general formula for the calculation of atomic photo-ionization cross-sections," Monthly Notices of the Roy. Astron. Soc., 120, 121-151 (1960).

26. Richter, J., "On the oscillator strengths of multiplets of neutral nitrogan," Zeitschrift fur Astrophysik, 51, 177-186 (1961).

27. Allen, C.W., "Astrophysical quantities," University of London Athlone Press (1955).

28. Feldman, S., "Hypersonic gas dynamic charts for equilibrium air," Avco-Everett Research Laboratory Research Report 40, January 1957.

29. Gilmore, F.R., "Equilibrium composition and thermodynamic properties of air to 24,000°K," Rand Corporation, Santa Monica, California, RM-1543 (1955).

30. Branscomb, L.M., Burch, B.S., Smith, S.J. and Geltman, S., "Photodetachment cross-section and the electron affinity of atomic oxygen," Phys. Rev., 111, 504-513 (1958).

31. Taylor, R.L., "Continuum infrared radiation from high temperature air and nitrogen," To be published as an Avco-Everett Research Laboratory Research Report.

32. Boldt, G., "The recombination and 'minus' continua of oxygen atoms," Z. für Physik, 154, 319-329 (1959).

33. Boldt, G., "The recombination and 'minus' continua of nitrogen atoms," Z. für Physik, 154, 330-338 (1959).

34. Wray, K.L., "Chemical kinetics of high temperature air," ARS Reprint 1975-61, August 1961.

35. Allen, R.A., Keck, J.C. and Camm, J.C., "Non-Equilibrium radiation from shock heated nitrogen and a determination of the recombination rate," Avco-Everett Research Laboratory Research Report 110, June 1961; also, Phys. of Fluids, 5, 284-291 (1962).

36. Hammerling, P., Teare, J.D. and Kivel, B., "Theory of radiation from luminous shock waves in nitrogen," Avco-Everett Research Laboratory Research Report 49, December 1959; also, Phys. of Fluids, 2, 422-426 (1959).

37. Treanor, C.E. and Marrone, P.V., "Vibration and dissociation coupling behind strong shock waves," Cornell Aeronautical Laboratory, Buffalo, N.Y., presented at the Symposium on Dynamics of Manned Lifting Planetary Entry, October 29-31, 1962, Philadelphia, Pennsylvania.

38. Wray, K.L., "A shock tube study of the coupling of the O_2-Ar rates of dissociation and vibrational relaxation," Avco-Everett Research Laboratory Research Report 125, January 1962; also, J. Chem. Phys., 37, 1254-1263 (1962).

39. Massey, H.S.W. and Burhop, E.H.S., Electronic and Ionic Impact Phenomena (Clarendon Press, London, 1952).

40. Faizullov, F.S., Sobolev, N.N. and Kudryavtsev, E.M., "Spectroscopic investigation of the state of the gas behind a shock wave, III," Optics and Spectroscopy, 8, 400-404 (1960).

41. Clouston, J.G., Gaydon, A.G. and Hurle, I.R., "Temperature measurements of shock waves by spectrum-line reversal.II - A double-beam method," Proc. Roy. Soc., A, 252, 143-155 (1959).

42. Gaydon, A.G. and Hurle, I.R., "Measurements of times of vibrational relaxation and dissociation behind shock waves in N_2, O_2, CO, CO_2, and H_2," Eighth Symposium (International) on Combustion, Pasadena, California (Williams and Wilkins, Baltimore, Maryland, 1962) p. 309-318.

43. Treanor, C.E., "Radiation at hypersonic speeds," ARS Preprint 1978-61, August 1961.

44. Feldman, S., "Trails of axisymmetric hypersonic blunt bodies flying through the atmospere," Avco-Everett Research Laboratory Research Report 82, December 1959.

45. Whalen, R.J., "Viscous and inviscid non-equilibrium gas flows," IAS Reprint 61-23, January 1961.

46. Lick, W., "Inviscid flow of a reacting mixture of gases around a blunt body," J. Fluid Mech., 7, 128-144 (1960).

47. Wurster, W.H. and Marrone, P.V., "Study of infrared emission in heated air," Cornell Aeronautical Laboratory Report QM 1373-A-4, July 1961.

48. Minzner, R.A., Champion, K.S.W. and Pond, H.L., "The ARDC Model Atmosphere, 1959," Air Force Cambridge Research Center TR 59-267, August 1959.

49. Wick, B.H., "Radiative heating of vehicles entering the Earth's atmosphere," Ames Research Center, presented to the Fluid Mechanics Panel of Advisory Group for Aeronautical Research and Development, Brussels, Belgium, April 3-6, 1962, NASA, Washington, D.C.

50. Hall, J.G., Eschenroeder, A.Q. and Marrone, P.V., "Inviscid hypersonic airflows with coupled chemical reactions," IAS Paper 62-67, January 1962.